NASA
Technical
Paper
2024

June 1982

Longitudinal Aerodynamic Characteristics of an Elliptical Body With a Horizontal Tail at Mach Numbers From 2.3 to 4.63

Barrett L. Shrout
and A. Warner Robins

NASA

NASA Technical Paper 2024

1982

Longitudinal Aerodynamic Characteristics of an Elliptical Body With a Horizontal Tail at Mach Numbers From 2.3 to 4.63

Barrett L. Shrout
Langley Research Center
Hampton, Virginia

A. Warner Robins
Kentron International, Inc.
Hampton, Virginia

National Aeronautics and Space Administration

Scientific and Technical Information Branch

SUMMARY

An investigation was conducted in the Langley Unitary Plan Wind Tunnel to determine longitudinal aerodynamic characteristics of a configuration consisting of an elliptical body with an in-plane horizontal tail. The tests were conducted at Mach numbers of 2.3, 2.96, 4.0, and 4.63.

In some cases, the configuration with negative tail deflections yielded higher values of maximum lift-drag ratio than did the configuration with an undeflected tail. This was due to body upwash acting on the tail and producing an additional lift increment with essentially no drag penalty.

Linear theory methods used to estimate some of the longitudinal aerodynamic characteristics of the model yielded results which compared well with experimental data for all Mach numbers in this investigation and for both small angles of attack and larger angles of attack where nonlinear (vortex) flow phenomena were present.

INTRODUCTION

For a number of years the National Aeronautics and Space Administration has been investigating the aerodynamic characteristics of bodies with elliptical cross sections. Included in these investigations were families of bodies with variations in ellipticity (ref. 1) and body-tail combinations. These body-tail combinations were either research configurations (ref. 2) or missile concepts (refs. 3 and 4). An elliptical body, with its major axis in the horizontal plane, has several advantages over a body of revolution. These advantages include more volume for a given vertical dimension or, conversely, a smaller vertical dimension for a given volume. This smaller vertical dimension may be used to produce missile configurations that are more adaptable to conformal carriage on aircraft. In addition, the planform of a body with an elliptical cross section provides a more efficient lifting surface than a body of circular cross section (with the same area distribution), and may reduce the wing size requirements for a cruise type missile or a hypersonic interceptor. The elliptical body also has greater lateral and directional stability, which may be utilized in configuration design.

As part of this continuing investigation of bodies with elliptical cross sections, a test was conducted in the Langley Unitary Plan Wind Tunnel at Mach numbers from 2.3 to 4.63 of a model with an elliptical cross-section body with an in-plane horizontal tail. The purpose of the wind-tunnel test was to obtain data on a simple body-tail configuration to provide an insight into the fundamental longitudinal aerodynamic characteristics of elliptical body-tail combinations. The use of an in-plane horizontal tail in contrast to tri-tail and quad-tail arrangements of some earlier investigations aids in the determination of body-tail effects by eliminating the mutual interference between the tails.

The theoretical longitudinal aerodynamic characteristics of the body-tail configuration were also obtained, using various linear theory techniques. These techniques, which are generally considered valid in the Mach number range from 1.3 to approximately 3.0, have been used with some success up to Mach number 4.63

(ref. 5). One of the purposes of this investigation was to explore the applicability of these linear methods to this type of configuration at Mach numbers above 3.0.

The wind-tunnel tests and theoretical predictions were conducted for Mach numbers of 2.3, 2.96, 4.0, and 4.63 at a nominal Reynolds number of 6.56×10^6 per meter (2.0×10^6 per foot).

SYMBOLS

Lift and drag data are referenced to the stability-axis system while moment data are referenced to the body-axis system. The moment reference center for the model is located 49.81 cm (19.61 in.) from the model nose on the model horizontal reference line.

The model was designed and built and data were reduced using U.S. Customary Units. Data are presented in SI Units with U.S. Customary Units in parentheses.

A cross-section area

A_{max} maximum cross-section area, 108.13 cm^2 (16.76 in^2)

C_D drag coefficient, $\frac{Drag}{qS}$

$C_{D,b}$ base drag coefficient, $\frac{Base\ drag}{qS}$

$C_{D,c}$ chamber drag coefficient, $\frac{Chamber\ drag}{qS}$

$C_{D,f}$ skin-friction drag coefficient

$C_{D,w}$ wave drag coefficient

$C_{D,o}$ $= C_{D,w} + C_{D,f}$

C_L lift coefficient, $\frac{Lift}{qS}$

C_{L_α} lift-curve slope at $\alpha = 0$, per deg

C_m pitching-moment coefficient, $\frac{Pitching\ moment}{qS\bar{c}}$

ΔC_D drag increment due to addition of tail

$\Delta C_D / \Delta C_L^2$ drag due to lift factor

ΔC_L lift increment due to addition of tail

$\partial C_m / \partial C_L$ longitudinal stability parameter at $C_L = 0$

$\partial C_m/\partial \delta_t$	pitching-moment effectiveness of horizontal tails at $C_L = 0$, per deg
$\bar{c}$	reference chord, 19.96 cm (7.86 in.)
L/D	lift-drag ratio
M	Mach number
q	free-stream dynamic pressure, Pa (psf)
S	wing reference area, 810.115 cm^2 (125.568 in^2)
x	distance from model nose, cm (in.)
x_{max}	maximum x distance from nose, 82.14 cm (32.34 in.)
y	spanwise distance from centerline, cm (in.)
α	angle of attack, deg
δ_t	tail deflection angle (positive trailing edge down), deg

Subscript:

max	maximum

MODELS AND INSTRUMENTATION

A sketch of the model is shown in figure 1 and photographs of the model installed in the Unitary Plan Wind Tunnel are shown in figure 2. The planform of the body is defined by the following equations:

$$x, \text{ leading edge} = \frac{0.3(K_1 y + 2.0)^2 - 1.2}{K_1}$$

$$y, \text{ leading edge} = \frac{[(K_1 x + 1.2)/0.3]^{1/2} - 2}{K_1}$$

where K_1 equals 1.077 for dimensions in centimeters and 2.737 for dimensions in inches. The area distribution for the body is defined by the equation

$$A(x) = \frac{-(K_1 x)^3/1200 + (K_1 x)^2/15 + K_1 x}{K_2}$$

where K_2 is 1.161 for dimensions in centimeters and 7.491 for dimensions in inches. The equation for the area distribution applies for the region $x = 0$ to $x = 55.756$ cm (21.951 in.). At this point, the slope of the area distribution is zero and the theoretical area distribution remains constant to the end of the body. However, the outboard part of the model body aft of $x = 58.49$ cm (23.03 in.) was modified to provide an attachment region for the horizontal tail, resulting in a decrease in the body cross-section area, as shown in the nondimensionalized normal area distribution in figure 3. The horizontal tail attachment region on the model body was contoured so that, as the horizontal tail was rotated about its swept hinge line, the inboard edge of the tail maintained contact with the body side until the tail was deflected more than approximately 4°, when it began to unport. The horizontal tail had 4-percent-thick circular-arc sections.

The base region of the model body was recessed 2.54 cm (1 in.) as shown in figure 1 to provide a quiescent region for taking base pressure measurements. Base pressure was measured by four tubes located in the recessed area, close to, but not touching, the model base. Chamber pressure was measured by two tubes located in the balance-sting cavity. The six pressure tubes were attached to the model support sting and routed to pressure transducers which were located outside the tunnel test section.

Forces and moments were measured by means of a six-component strain-gage balance which was contained within the model and connected by a supporting sting to the permanent model-actuating systems in the tunnel.

TEST CONDITIONS AND CORRECTIONS TO DATA

Tests were conducted in the Langley Unitary Plan Wind Tunnel at Mach numbers of 2.3, 2.96, 4.0, and 4.63. The tests were conducted under the following conditions of pressure, temperature, and Reynolds number:

Mach number	Stagnation pressure		Stagnation temperature		Reynolds number	
	kPa	psf	K	°F	per meter	per foot
2.30	73.065	1526	338.71	150	6.56×10^6	2.0×10^6
2.96	97.963	2046	338.71	150	6.20	1.89
4.00	188.600	3939	352.56	175	6.56	2.0
4.63	252.568	5275	352.56	175	6.56	2.0

Reynolds number for the test at $M = 2.96$ was about 5 percent lower than for the remainder of the test Mach numbers due to an inadvertent selection of an incorrect stagnation pressure. The only effect this should have on the data is an increase in measured drag for Mach number 2.96. The increase in C_D was estimated to be between 0.0001 and 0.0002.

The location of the transition from laminar to turbulent boundary-layer flow over the model was fixed by bands of No. 35 carborundum grit. One band was located 3.05 cm (1.20 in.) from the body apex around the nose and others were 1.40 cm (0.55 in.) back in a streamwise direction from the leading edge of the horizontal

tail. The required size and location of the transition bands were determined by the method of reference 6.

Corrections were made to the data for wind-tunnel flow angularity, balance component interactions, and sting deflections due to model loads. Base and chamber data were acquired simultaneously with all force data and the force data were adjusted to correspond to free-stream static pressure acting over the base and chamber area. Typical base-pressure drag increments are shown in figure 4. The base-pressure drag increment is essentially invariant with angle of attack at all Mach numbers except $M = 2.3$ where the base-pressure drag increases for angles of attack above 5°. Typical chamber-pressure drag increments are shown in figure 5, and behave in much the same manner as the base-pressure drag increments.

RESULTS AND DISCUSSION

The combined base-pressure and chamber-pressure drag corrections comprise a significant part of the minimum drag of the model, accounting for over 50 percent of the minimum drag at $M = 2.3$ and about 36 percent of the minimum drag at $M = 4.63$. The lift-drag ratios for the model are thus considerably larger as a result of the base-pressure and chamber-pressure drag corrections. The magnitude of the base-pressure and chamber-pressure drag corrections is not surprising since there is very little body closure on the model (see fig. 3). Although this may appear unrealistic from a configuration standpoint, it should be recognized that much of the base area would be required to accommodate a propulsion exhaust system.

The effects of the undeflected tail on the lift, drag, and pitching-moment characteristics of the model are shown in figure 6. The nonlinear behavior of the body lift curve, with a pronounced break at about 4°, is caused by the formation of upper surface vortices which generate additional lift on the body. The addition of the tail increases the slope of the lift curve and attenuates the nonlinearity due to the vortex formation. This can be attributed to a reduction in vortex strength over the aft part of the body, due to the presence of the tail, and flow separation from the tail at higher angles of attack.

For the moment center of this investigation, the body alone is unstable at all Mach numbers; however, pitch-down occurs at about 4° angle of attack, indicating that the resultant of the additional lift shown by the body lift curve is aft of the moment center. The addition of the horizontal tail results in a stable or neutrally stable configuration at $C_L = 0$; however, the effect of the tail on the body vortices reduces the vortex lift on the aft part of the body, producing pitch-up at about 4° angle of attack.

The effects of horizontal tail deflections on the static longitudinal aerodynamic characteristics of the body-tail configuration are shown in figure 7. The increments in lift and pitching moment due to tail deflection tend to vary proportionally to the amount of tail deflection and to decrease with increasing Mach number. Minimum drag decreases with increasing Mach number and increases with increasing tail deflection.

Of particular interest is the fact that for Mach number 2.3, negative tail deflections up to -6° result in $(L/D)_{max}$ greater than for the configurations with undeflected tails. This effect can be observed up to Mach number 4.0 for smaller tail deflections. Thus, the positive increment in C_m for trimming the configuration is accompanied by an increase in $(L/D)_{max}$.

The incremental lift due to the horizontal tail is shown in figure 8. These data were extracted from figures 6 and 7. The solid line shows the lift increment between the body and body-tail with the tail undeflected. The dashed line shows the lift increment between the body and body-tail where $\alpha = -\delta_t$, that is, with the tail aligned with the free stream. The lift due to the tail at $\alpha = -\delta_t$ is due to the body upwash acting on the tail and is responsible for the increases in $(L/D)_{max}$ shown in figure 7 for the configurations with deflected tails. The reduction in the tail lift slope (the solid line in fig. 8) at the higher angles of attack contributes to the body-tail pitch-up shown in figures 6 and 7, and is probably due to flow separation on the tail.

Drag increments ΔC_D due to the tail are shown in figure 9. The variation in ΔC_D for $\delta_t = 0$ tends to be parabolic at the lower angles of attack but almost linear at the higher angles of attack, reflecting the loss of tail lift shown in figure 8. At $\alpha = 0$, the drag increment is composed of tail skin-friction drag plus the change in wave drag due to the addition of the tail. At $\alpha = -\delta_t$, there is essentially no drag associated with the lift generated by the tail. This reflects the fact that while the tail is at an effective angle of attack due to the body upwash field, the tail normal-force vector is perpendicular to the free stream (that is, there is no induced drag in the traditional sense of the normal-force vector tilted in the drag direction).

Comparison With Theory

As stated in the Introduction, one of the purposes of this investigation was to determine the applicability of some of the linear theory analytic methods in estimating the aerodynamic characteristics of an elliptical body in combination with a horizontal tail. Two techniques were used in evaluating the zero-lift wave drag of the model. The far-field method (ref. 7) uses the supersonic area rule and slender body theory, with the assumption that the Mach cone originating at the apex of a component will not intersect that component elsewhere. Thus, the assumption of the theory would be violated for a slender body at a sufficiently high Mach number, and the magnitude of error would be expected to increase as the Mach number increases.

The second technique is known as the near-field wave-drag program, described in reference 8. In this program, thickness pressures are calculated for various components and integrated to provide component wave drag, and their effect on other components is calculated. Although there are no geometric restraints peculiar to the method, the assumptions and limitations of linear theory still apply.

Skin-friction drag was calculated by the method of reference 9 and added to the estimates for zero-lift wave drag. The results are shown with experimental data in figure 10.

The far-field method estimates agree very well with the experimental data at $M = 2.3$ and 2.96. As expected, these estimates are in increasingly poor agreement above $M = 2.96$. The near-field method slightly overpredicts the drag at Mach number 2.3 but shows good agreement with the experimental data at the other Mach numbers.

Some of the other longitudinal aerodynamic characteristics of the model can be estimated by using the lifting surface evaluation method of reference 10. This method, also based on linear theory, calculates the zero-volume pressure distribution on the configuration for a lifting condition, integrates the pressures, and using superposition techniques, predicts drag due to lift, lift, and pitching-moment

characteristics for the configuration. A comparison between the theoretical aerodynamic characteristics and the experimental data is shown in figure 11. In constructing the theoretical drag polars, the near-field wave-drag values were used for all Mach numbers. The agreement between theory and experiment for the lift and drag data is exceptionally good. The discrepancy in the drag polars at $M = 2.3$ is primarily due to the error in predicting zero-lift wave drag. The stability level of the configuration is consistently overpredicted and the theoretical method cannot predict the pitch-up.

A comparison between theory and experiment for some longitudinal parameters as a function of Mach number is shown in figure 12. The lifting surface evaluation program was also used to estimate the effect of tail deflections. The tail effectiveness parameter $\partial C_m/\partial \delta_t$, which is essentially a measure of the amount of C_m generated by tail deflections, shows part of the results of that evaluation.

The agreement between theory and experiment for the tail effectiveness parameter, the drag-due-to-lift factor $\Delta C_D/\Delta C_L^2$, and the lift-curve slope C_{L_α} is quite good over the Mach number range. The longitudinal stability parameter, as previously mentioned, is consistently overpredicted. This error is perhaps not as significant as it may appear since it represents an error in the prediction of the center of lift of about 2 percent based on the overall length of the configuration.

Linear theory methods would not normally be expected to produce good results where there are significant nonlinear flow properties such as the upper surface vortices on the body of this configuration. However, the addition of the horizontal tail apparently modified the flow such that the lift and drag behaved in a nearly linear fashion. Although $M = 3.0$ is generally considered to be the upper limit for linear theory methods, for this configuration the methods are applicable up to $M = 4.63$, with the exception of the far-field wave-drag method.

Flow Visualization

Several techniques for flow visualization are used in the Langley Unitary Plan Wind Tunnel and three of these techniques were used in this investigation to obtain photographs to aid in interpreting the flow over the model. These included schlieren photographs, to observe the shock wave system generated by the model; fluorescent oil-flow photographs, to determine the surface flow characteristics over the model; and vapor-screen photographs, to observe the flow field about the model. Examples of these photographs are presented in figure 13 for angles of attack of 4° and 8°.

The schlieren photograph at the top of the figure is a side view of the model taken through the vertical bars supporting the tunnel sidewall windows. The oil-flow photograph in the middle of the figure shows a top view taken by two cameras mounted between the vertical bars. The vapor-screen photographs at the bottom of the figure are views from the upper left rear quadrant.

In the oil-flow photographs, the upper surface vortices, weakly developed at $\alpha = 4°$, are indicated by the dark streaks running from near the nose to the back end of the body. The dark streaks are caused by the higher velocity air of the vortex wiping the oil from the model surface. At $\alpha = 4°$, the vortices are not visible in the vapor-screen photographs; however, at $\alpha = 8°$, the dark areas at the model upper surface indicate the location of the vortices. For this angle of attack, the vortices appear much stronger in the oil-flow photographs. Flow separation on the hori-

zontal tail is also indicated at $\alpha = 8°$ by the buildup of light-colored oil along the trailing edge of the tail.

CONCLUDING REMARKS

An investigation was conducted in the Langley Unitary Plan Wind Tunnel at Mach numbers from 2.3 to 4.63 of a model consisting of an elliptical body and an in-plane horizontal tail. The following items are considered to be the most significant results of the investigation:

1. The base-pressure drag correction was on the order of one-half the uncorrected zero-lift drag of the model, and had a significant effect on the magnitude of the lift-drag ratios.

2. In some cases, the configuration with negative tail deflections yielded higher values of maximum lift-drag ratio than did the configuration with no tail deflection. This was due to body upwash acting on the tail which produced an additional lift increment with essentially no drag penalty.

3. Linear theory methods used to estimate some of the longitudinal aerodynamic characteristics of the model yielded results which compared well with experimental data for all Mach numbers in this investigation and for both small angles of attack and larger angles of attack where nonlinear (vortex) flow phenomena were present. These methods can therefore be used to provide guidance in designing configurations similar to the model in this investigation.

Langley Research Center
National Aeronautics and Space Administration
Hampton, VA 23665
May 6, 1982

REFERENCES

1. Fournier, Roger H.; Spencer, Bernard, Jr.; and Corlett, William A.: Supersonic Aerodynamic Characteristics of a Series of Related Bodies With Cross-Sectional Ellipticity. NASA TN D-3539, 1966.

2. Spencer, Bernard, Jr.; and Fournier, Roger H.: Supersonic Aerodynamic Characteristics of Hypersonic Low-Wave-Drag Elliptical-Body-Tail Combinations as Affected by Changes in Stabilizer Configuration. NASA TM X-2747, 1973.

3. Graves, Ernald B.: Aerodynamic Characteristics of a Monoplanar Missile Concept With Bodies of Circular and Elliptical Cross Sections. NASA TM-74079, 1977.

4. Graves, Ernald B.; and Robins, A. Warner: Supersonic Aerodynamic Trade Data for a Low-Profile Monoplanar Missile Concept. AIAA Paper 79-0222, Jan. 1979.

5. Jernell, Lloyd S.: Longitudinal Aerodynamic Characteristics of Wing-Body Models With Arrow, Delta, and Diamond Planforms at Mach Numbers From 2.3 to 4.63 and Comparisons With Theory. NASA TM X-1522, 1968.

6. Braslow, Albert L.; Hicks, Raymond M.; and Harris, Roy V., Jr.: Use of Grit-Type Boundary-Layer-Transition Trips on Wind-Tunnel Models. Conference on Aircraft Aerodynamics, NASA SP-124, 1966, pp. 19-36. (Also available as NASA TN D-3579.)

7. Harris, Roy V., Jr.: An Analysis and Correlation of Aircraft Wave Drag. NASA TM X-947, 1964.

8. Middleton, W. D.; Lundry, J. L.; and Coleman, R. G.: A Computational System for Aerodynamic Design and Analysis of Supersonic Aircraft. Part 2 - User's Manual. NASA CR-2716, 1976.

9. Sommer, Simon C.; and Short, Barbara J.: Free-Flight Measurements of Turbulent-Boundary-Layer Skin Friction in the Presence of Severe Aerodynamic Heating at Mach Numbers From 2.8 to 7.0. NACA TN 3391, 1955.

10. Middleton, Wilbur D.; and Carlson, Harry W.: Numerical Method of Estimating and Optimizing Supersonic Aerodynamic Characteristics of Arbitrary Planform Wings. J. Aircr., vol. 2, no. 4, July-Aug. 1965, pp. 261-265.

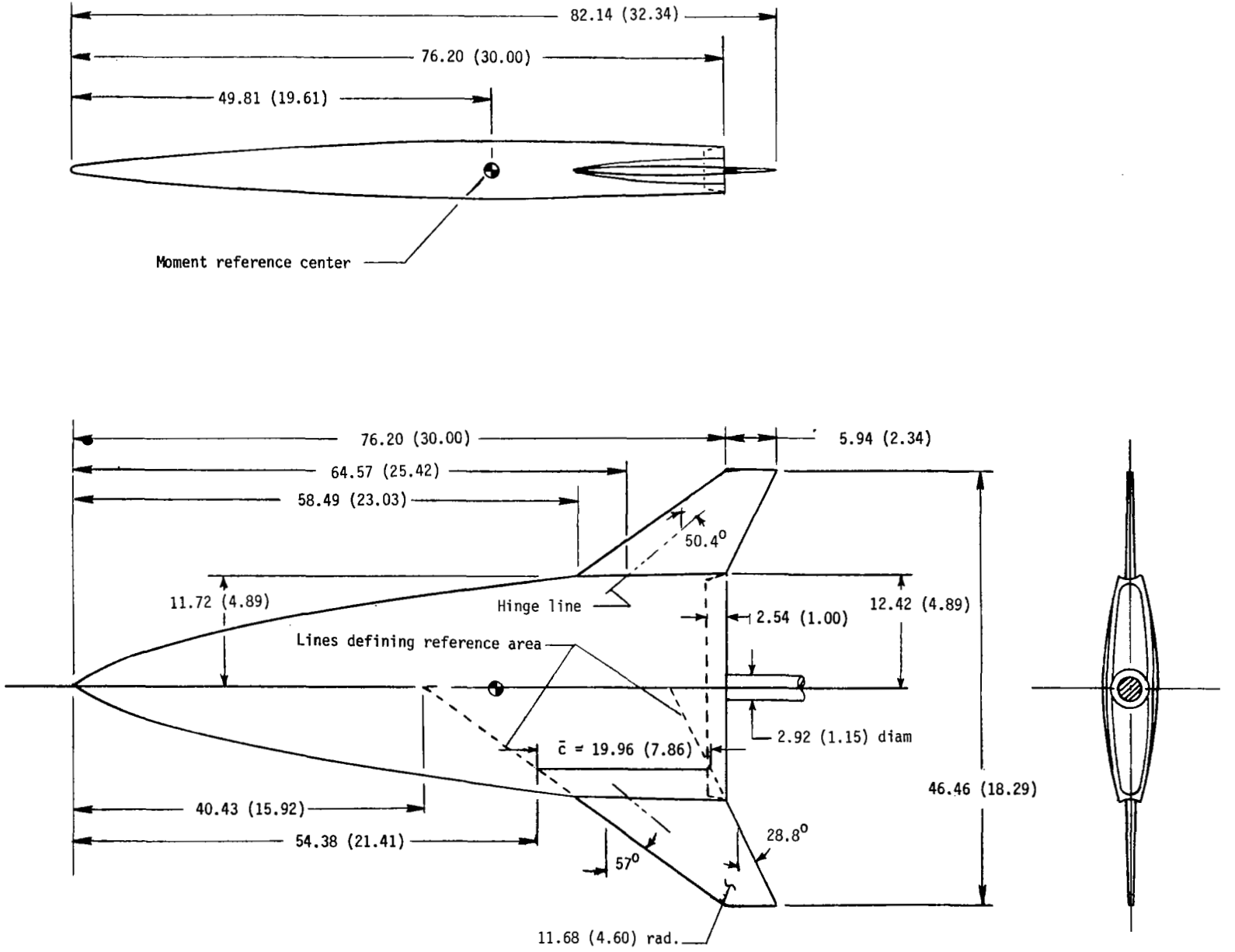

Figure 1.- Three-view sketch of model. All linear dimensions are in centimeters (inches).

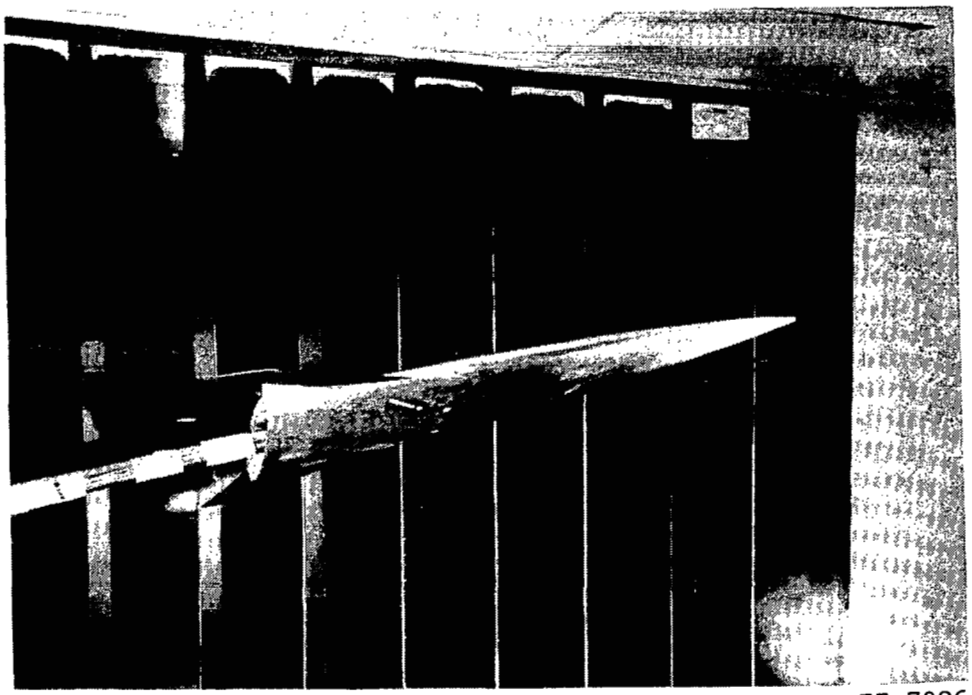

L-77-7086

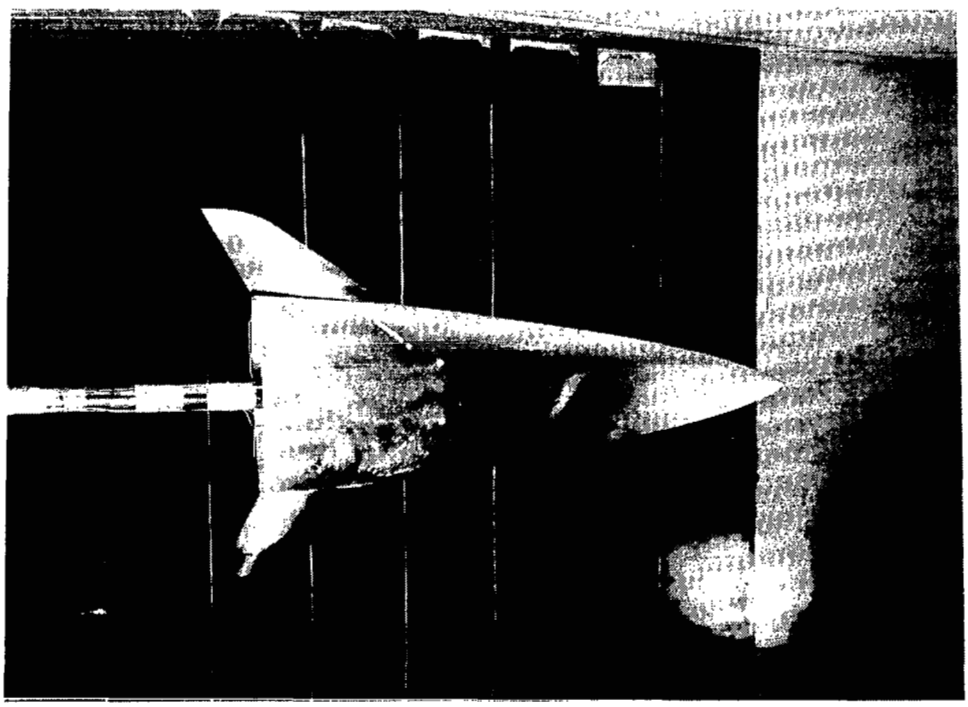

L-77-7088

Figure 2.- Photographs of model installed in Langley Unitary Plan Wind Tunnel. $\delta_t = -4°$.

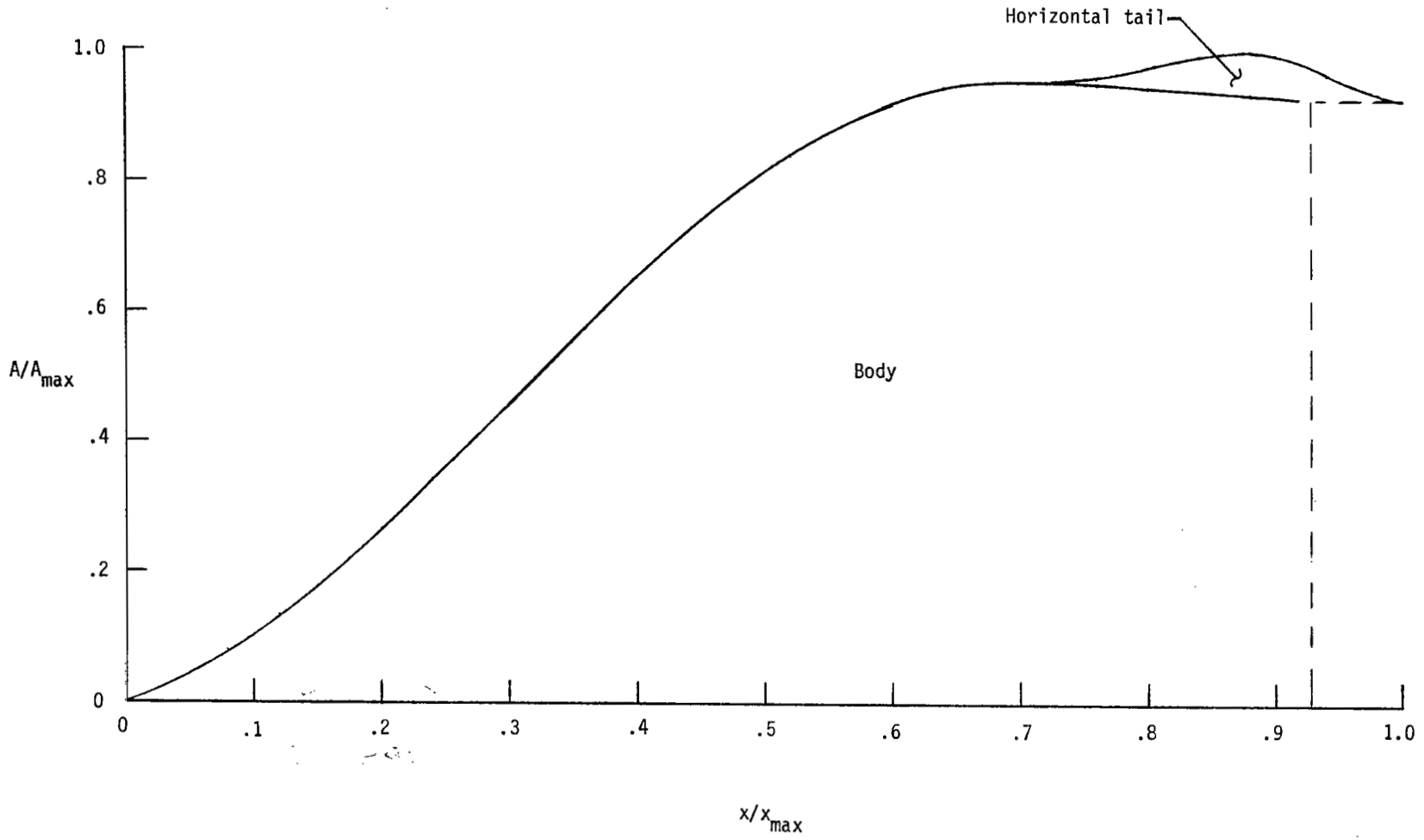

Figure 3.- Nondimensionalized normal area distribution for model.

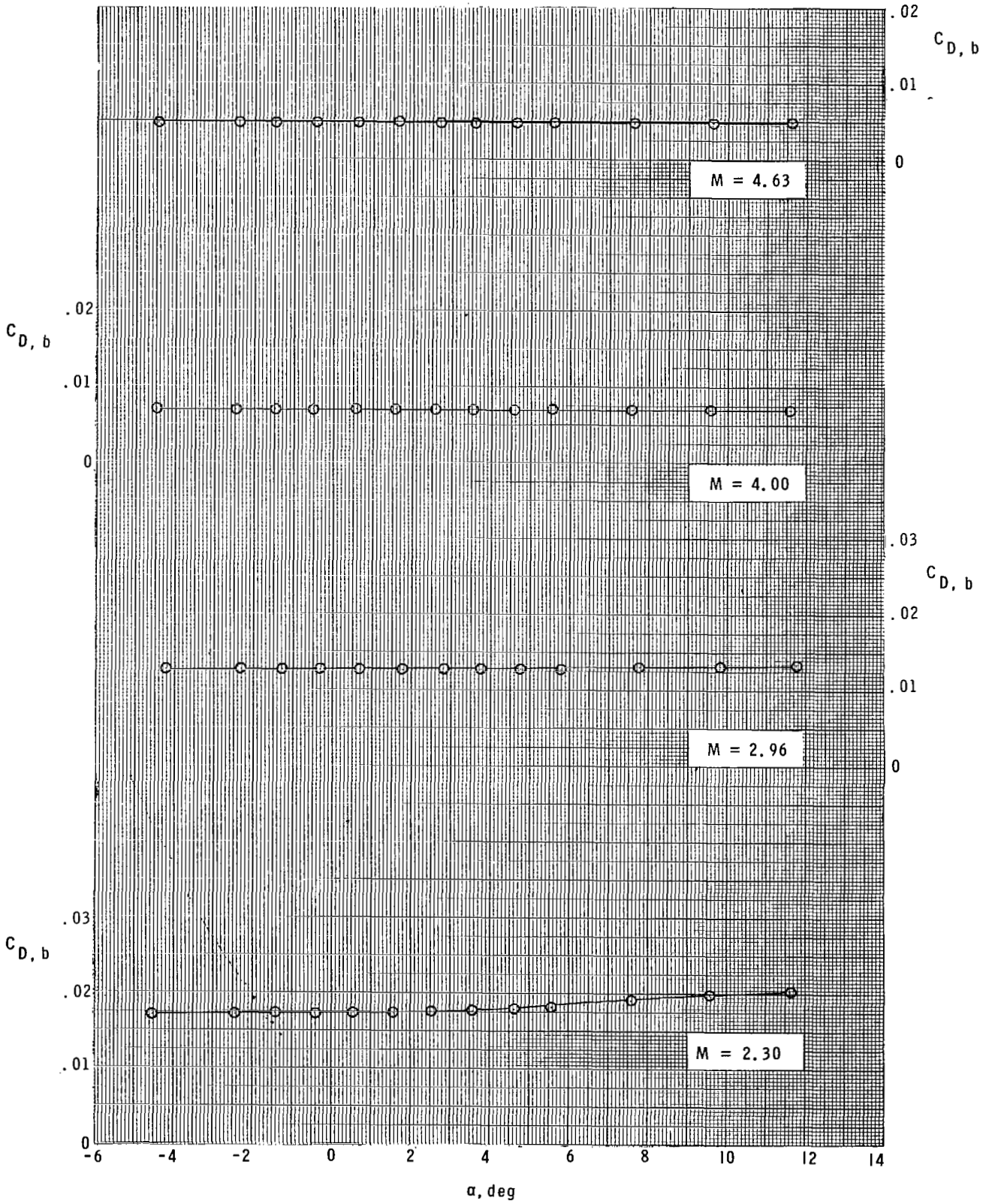

Figure 4.- Variation of base-pressure drag with angle of attack for various Mach numbers.

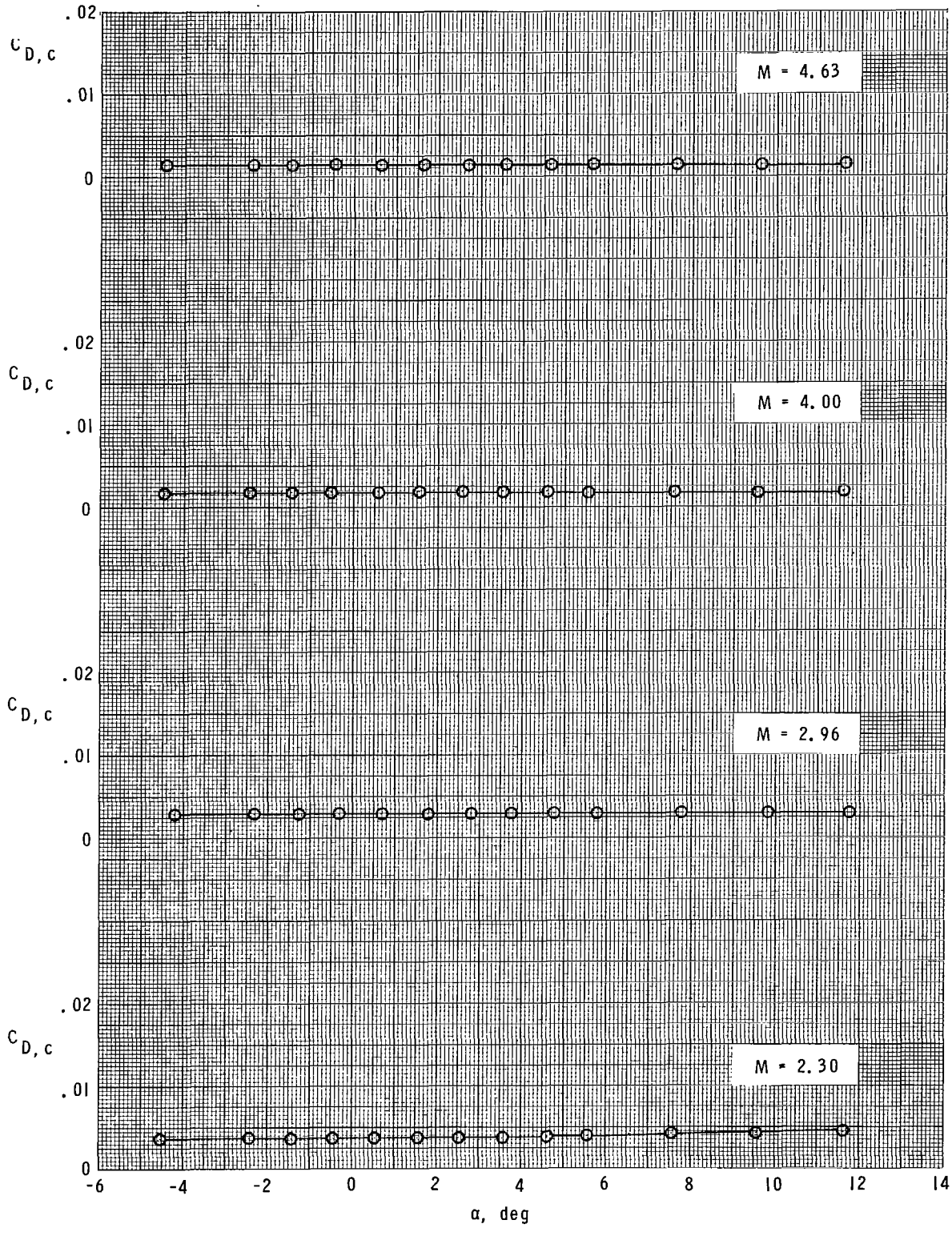

Figure 5.- Variation of chamber-pressure drag with angle of attack for various Mach numbers.

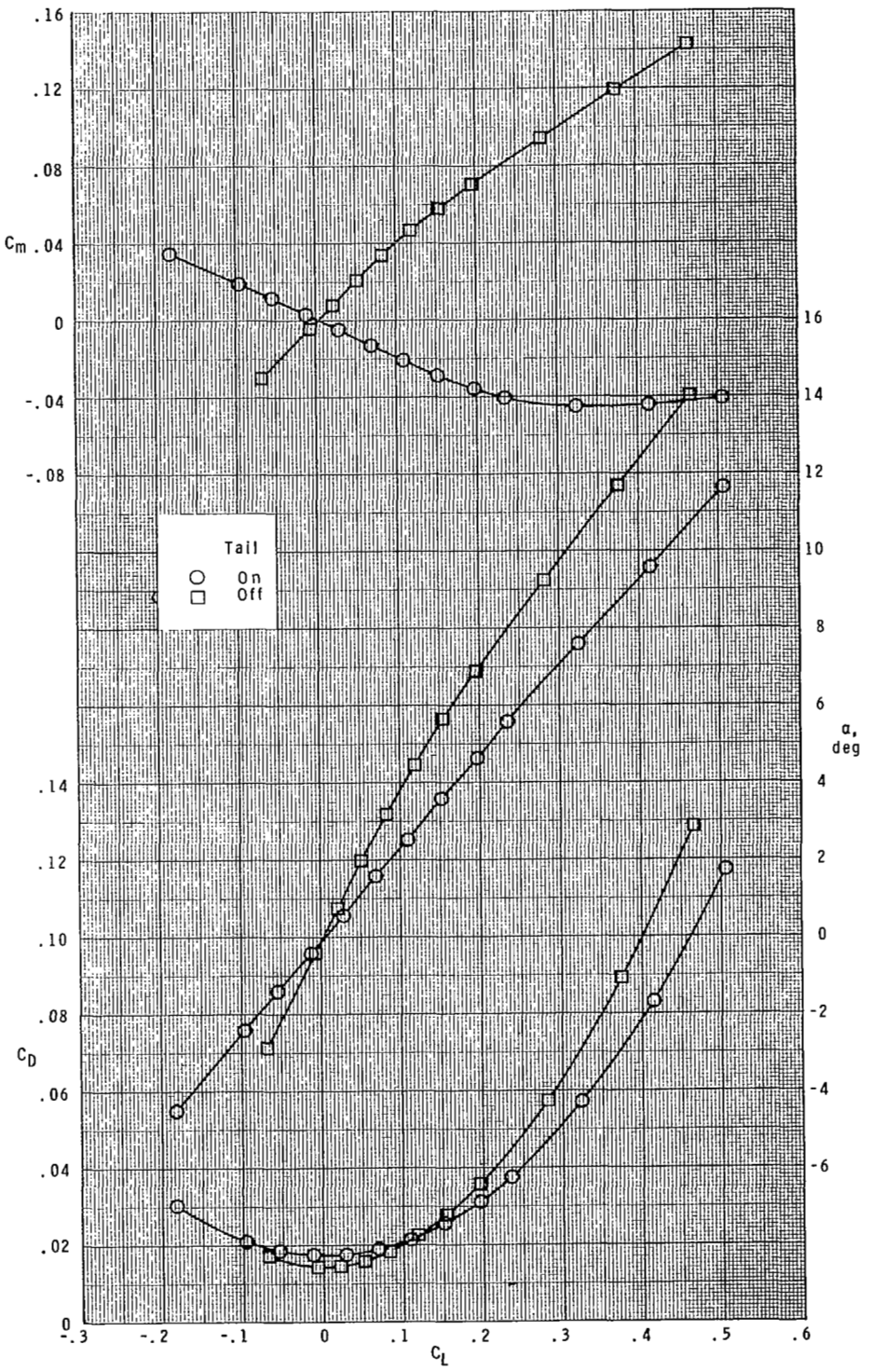

(a) M = 2.30.

Figure 6.- Longitudinal aerodynamic characteristics of model with tail on and off. $\delta_t = 0$.

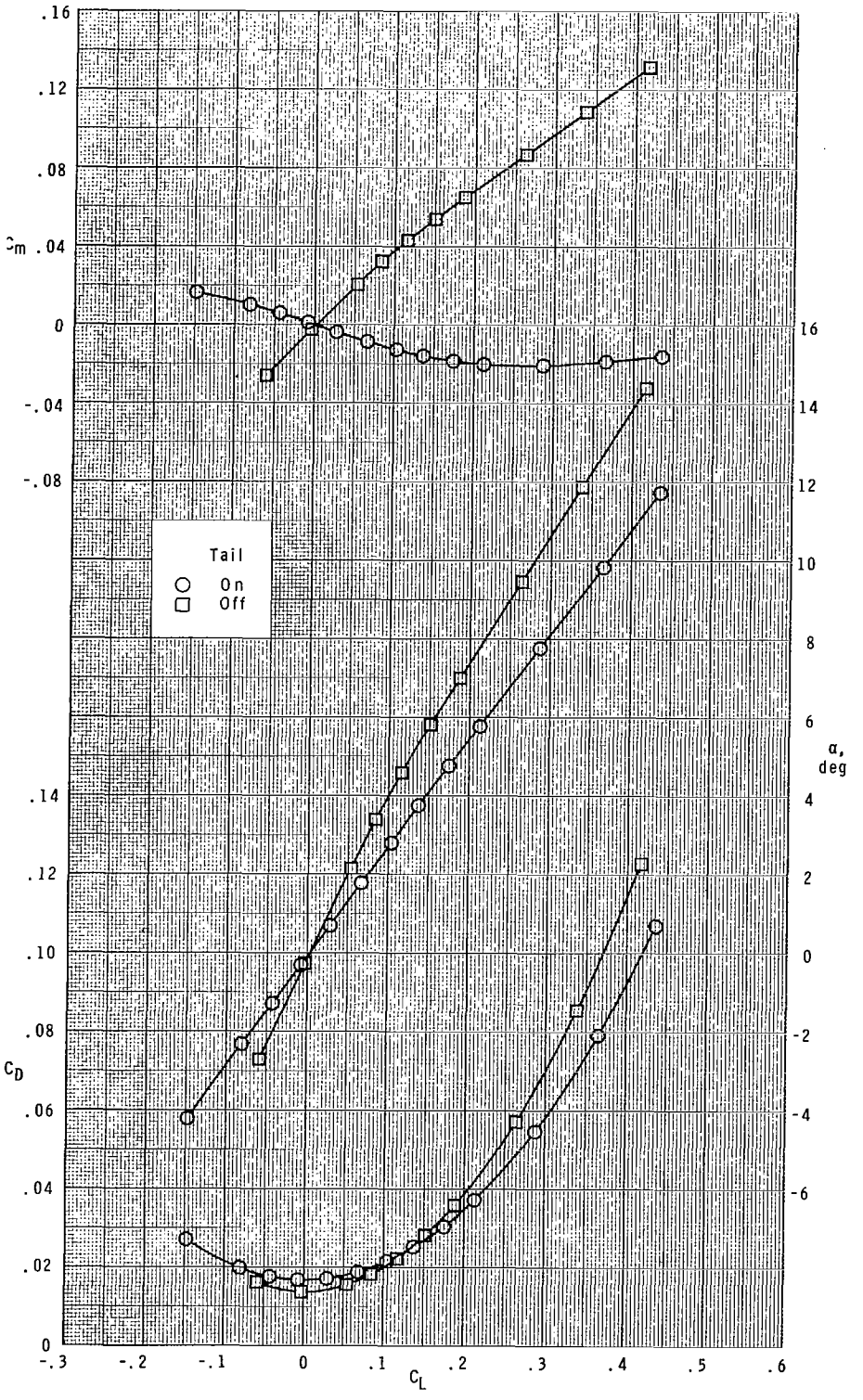

(b) M = 2.96.

Figure 6.- Continued.

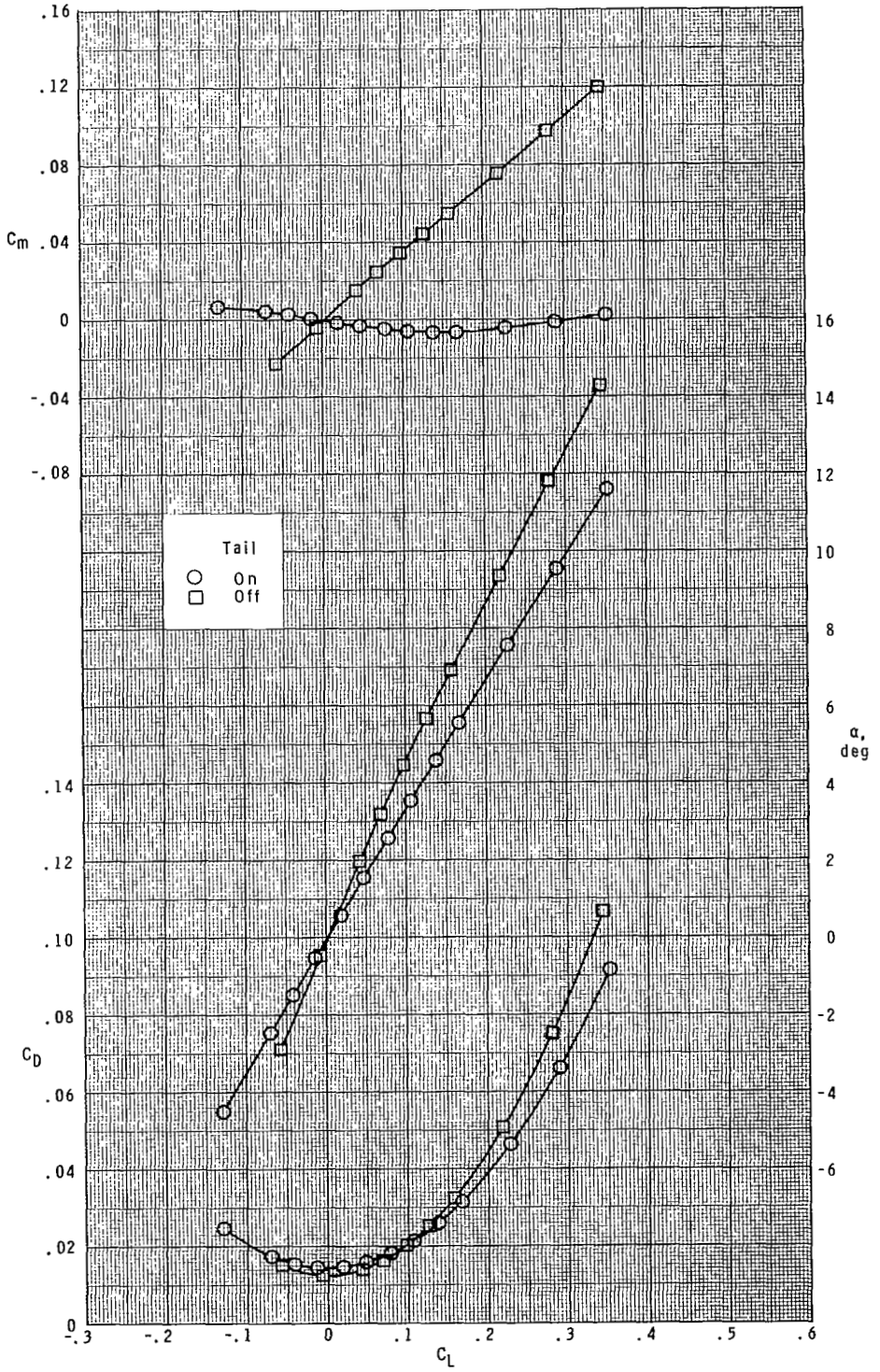

(c) M = 4.00.

Figure 6.- Continued.

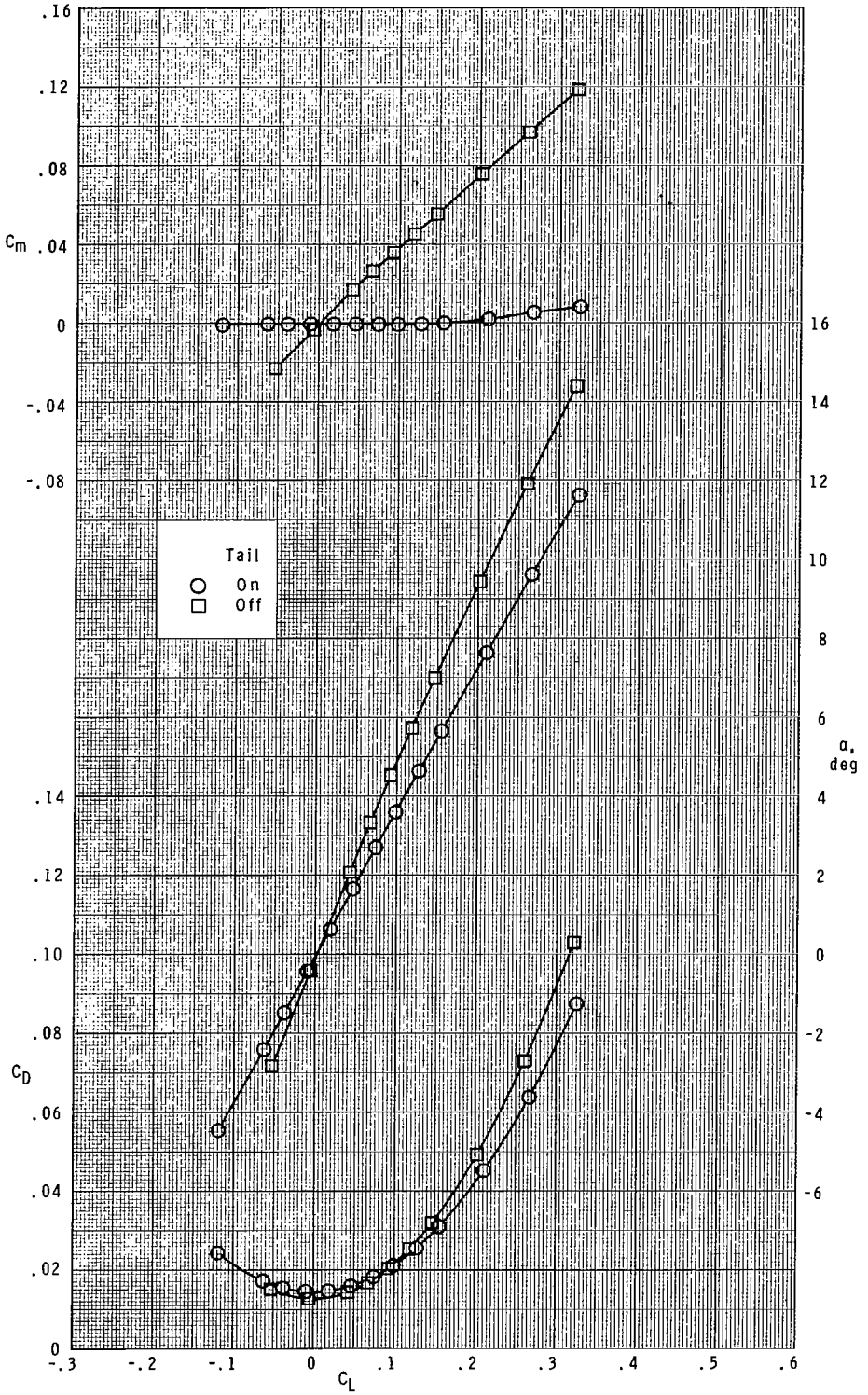

(d) M = 4.63.

Figure 6.- Concluded.

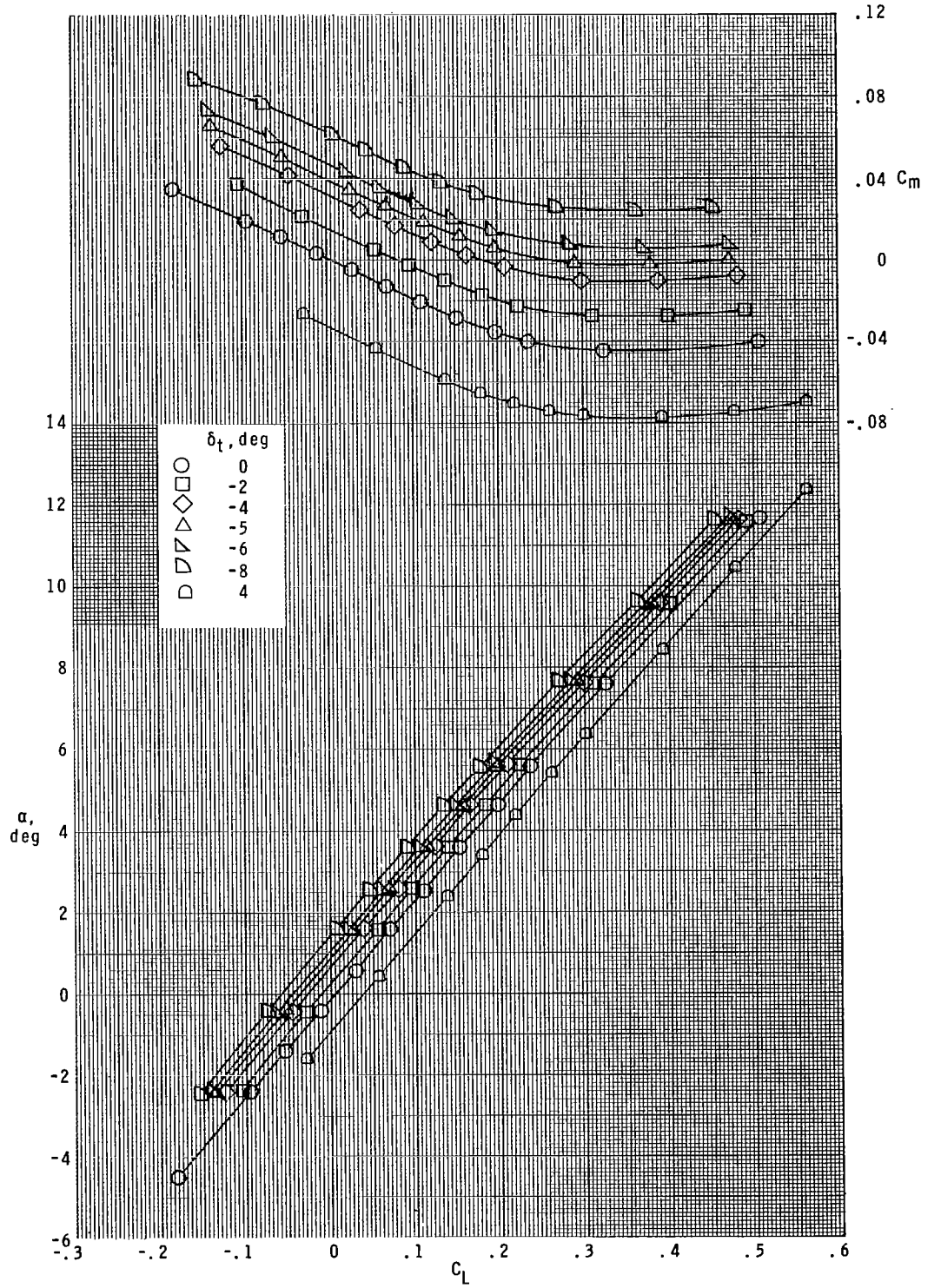

(a) M = 2.30.

Figure 7.- Effects of horizontal tail deflections on longitudinal aerodynamic characteristics of model.

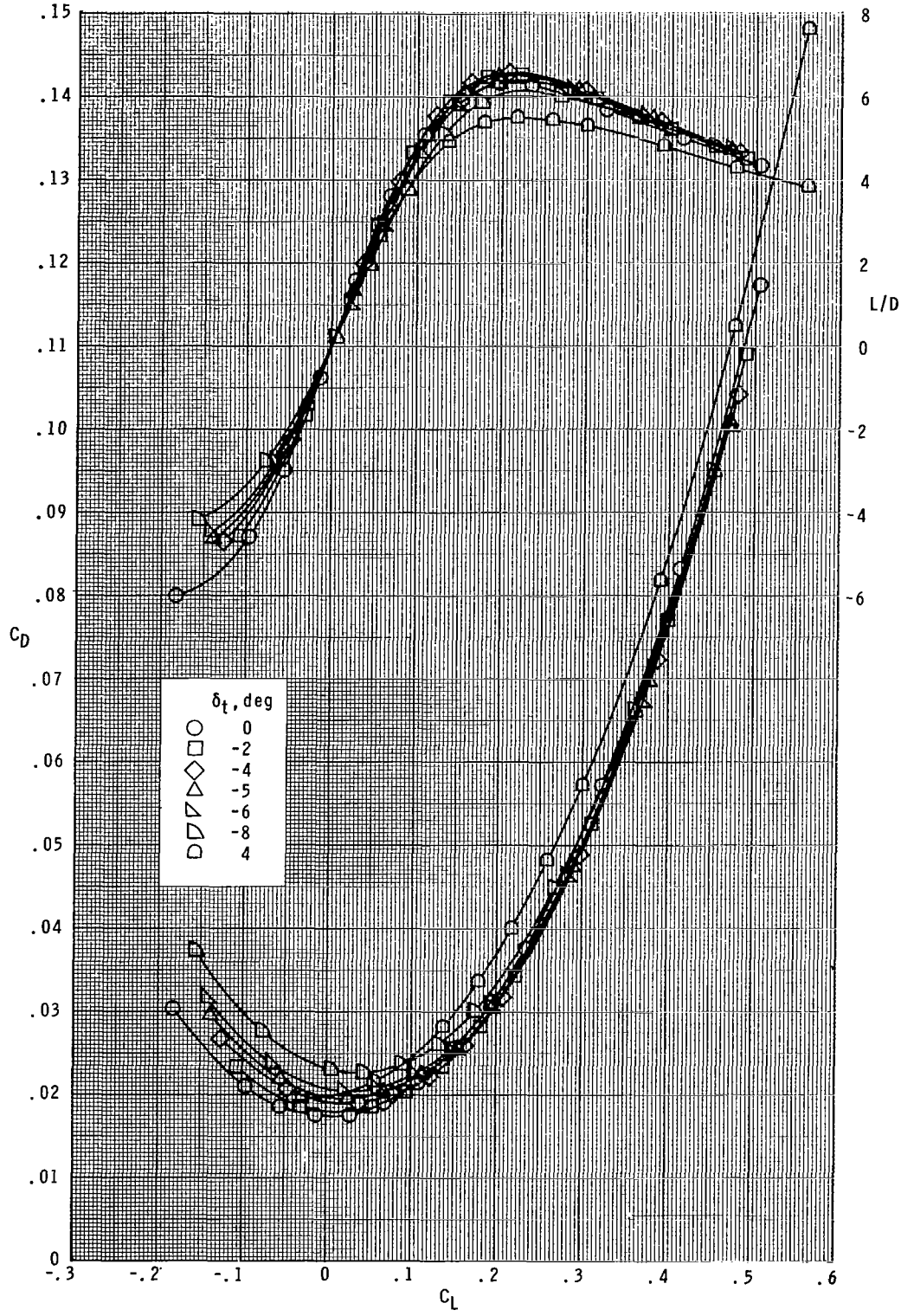

(a) Concluded.

Figure 7.- Continued.

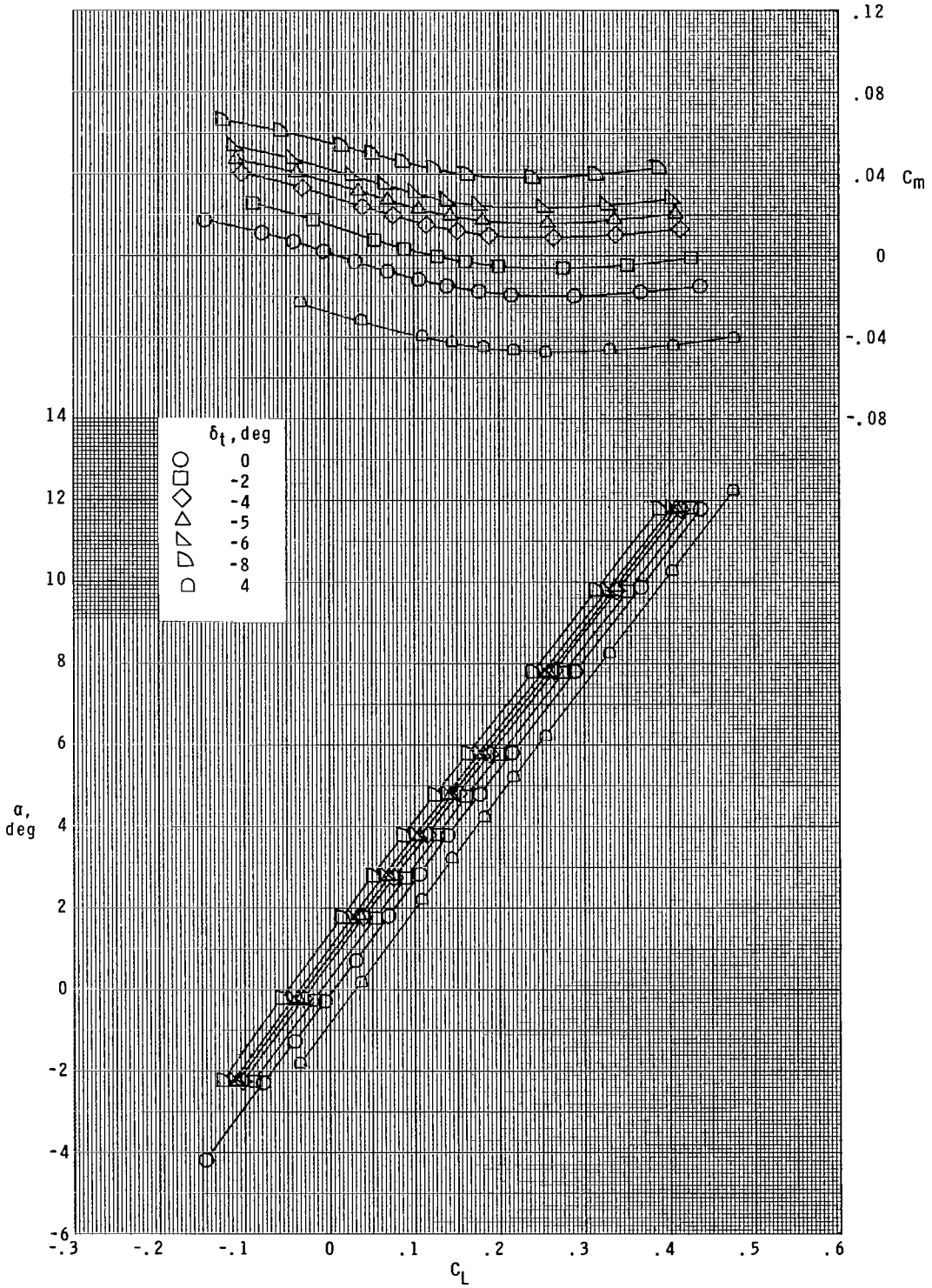

(b) M = 2.96.

Figure 7.- Continued.

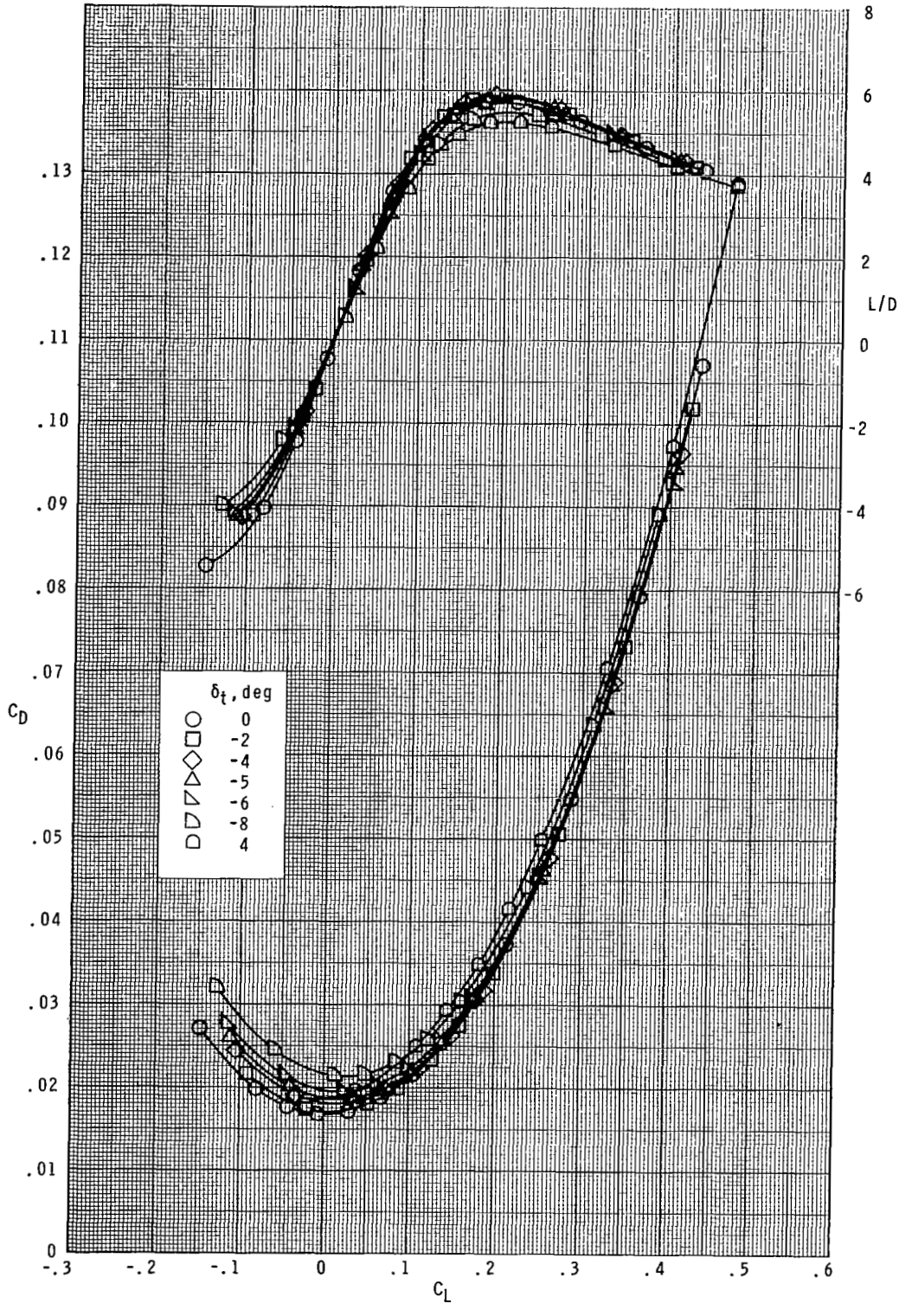

(b) Concluded.

Figure 7.- Continued.

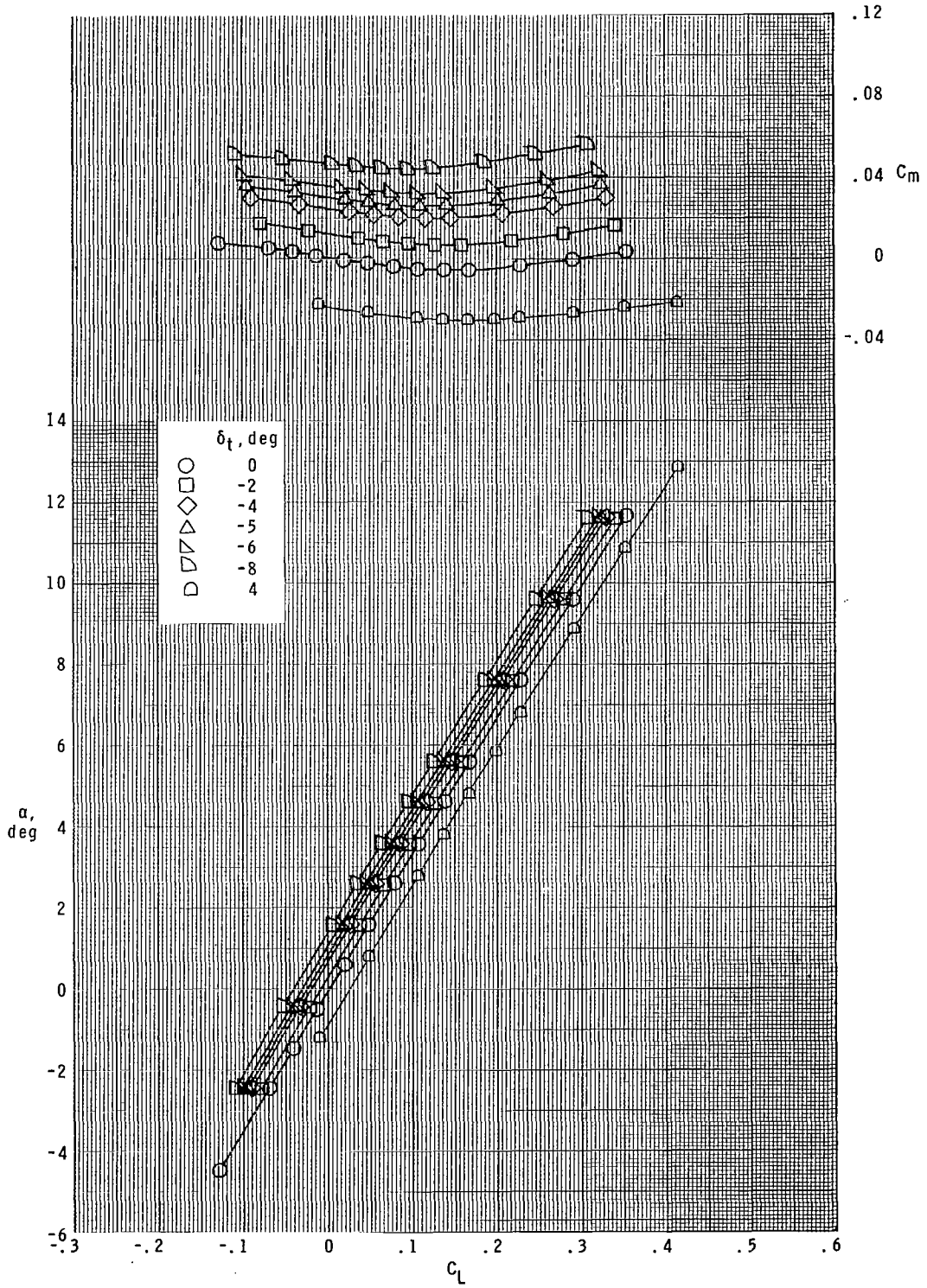

(c) M = 4.00.

Figure 7.- Continued.

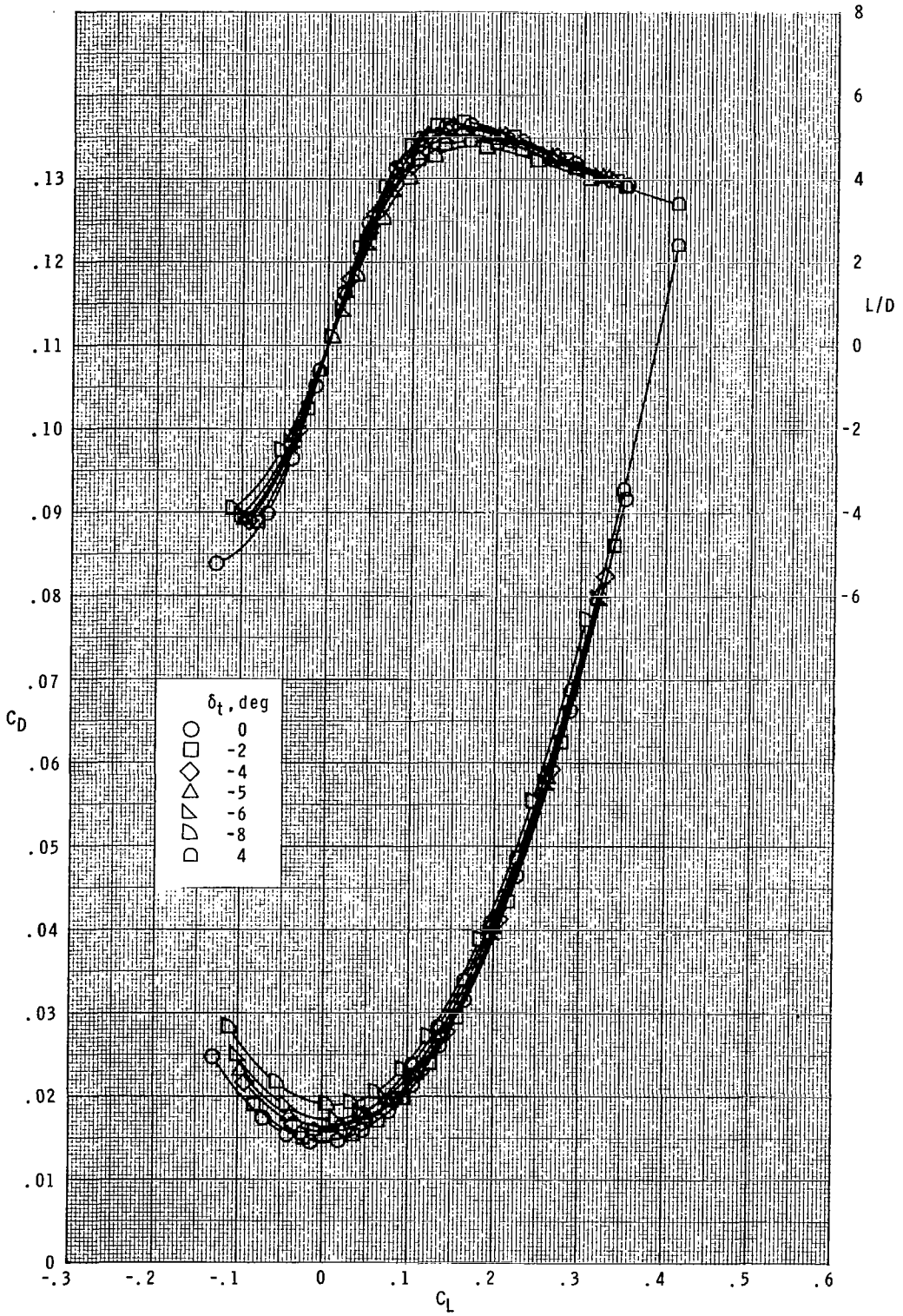

(c) Concluded.

Figure 7.- Continued.

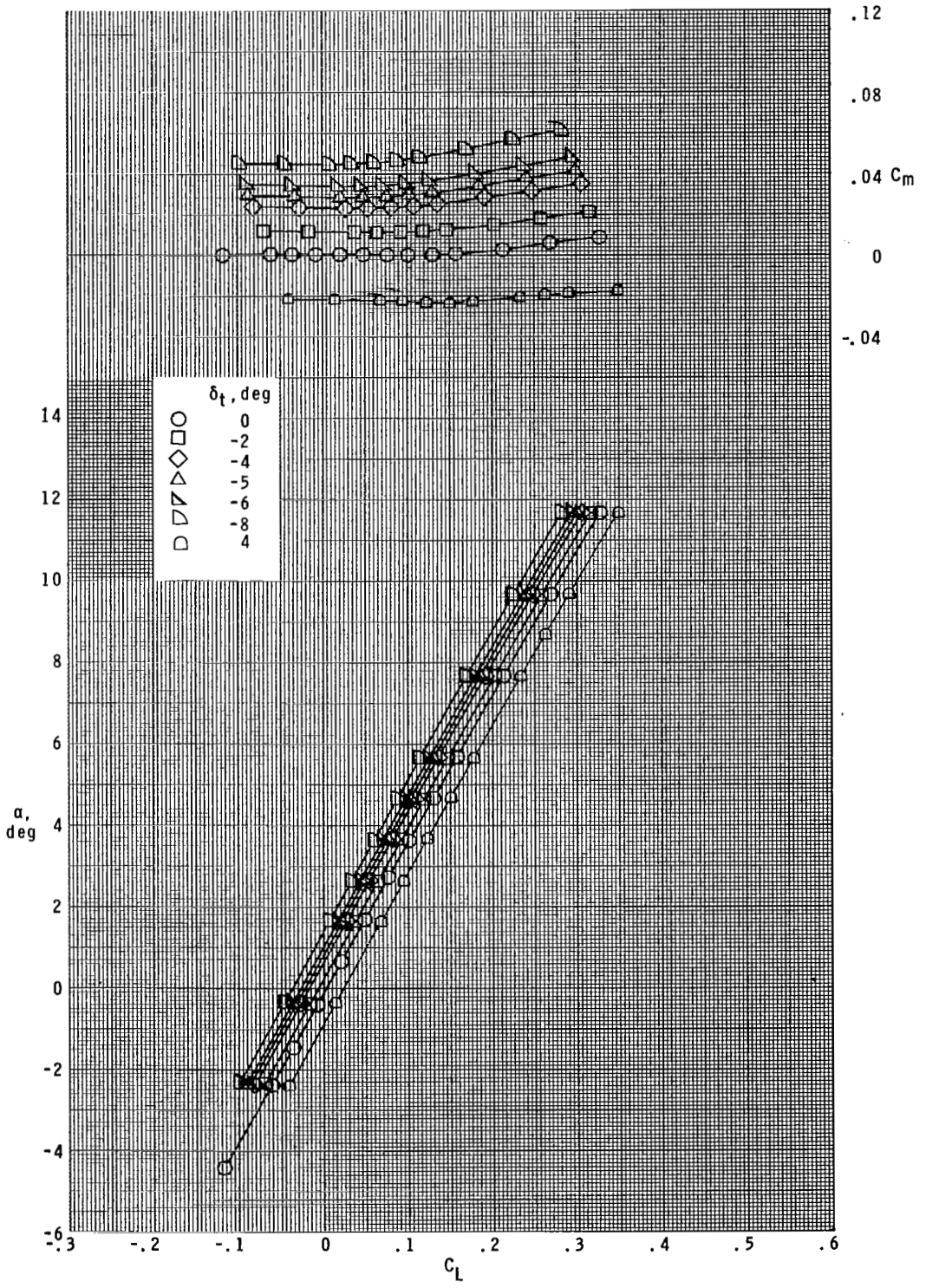

(d) M = 4.63.

Figure 7.- Continued.

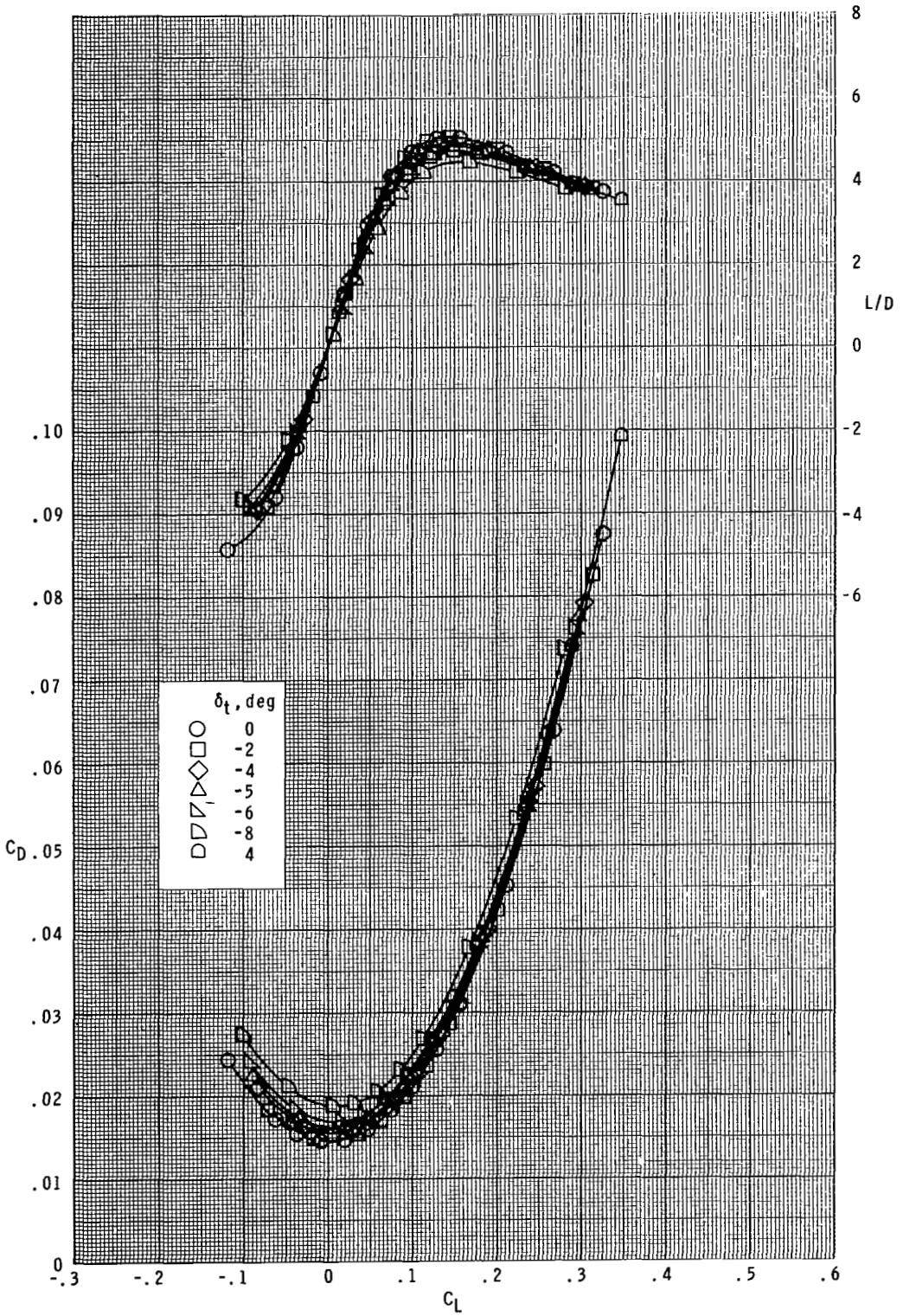

(d) Concluded.

Figure 7.- Concluded.

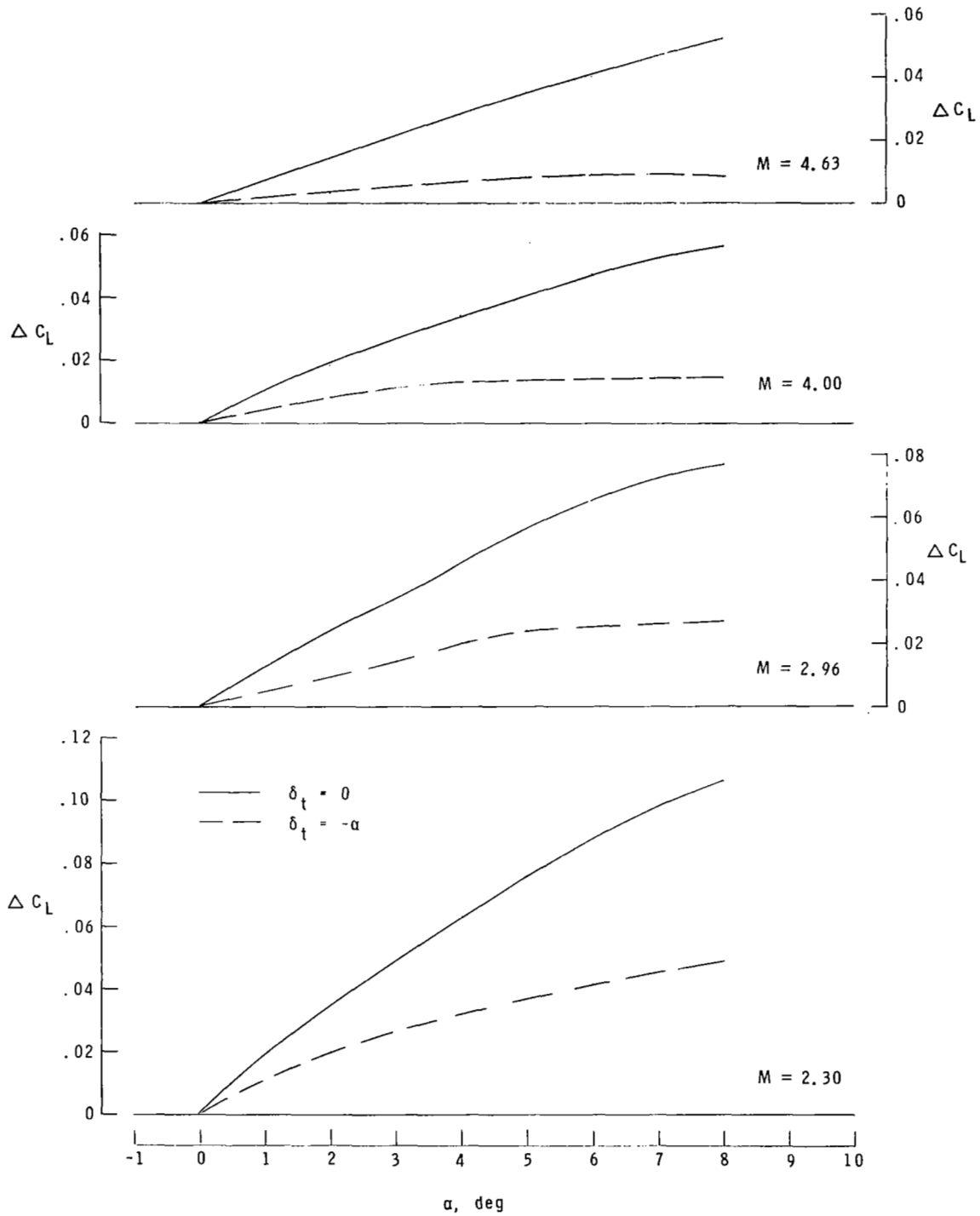

Figure 8.- Incremental lift due to horizontal tail.

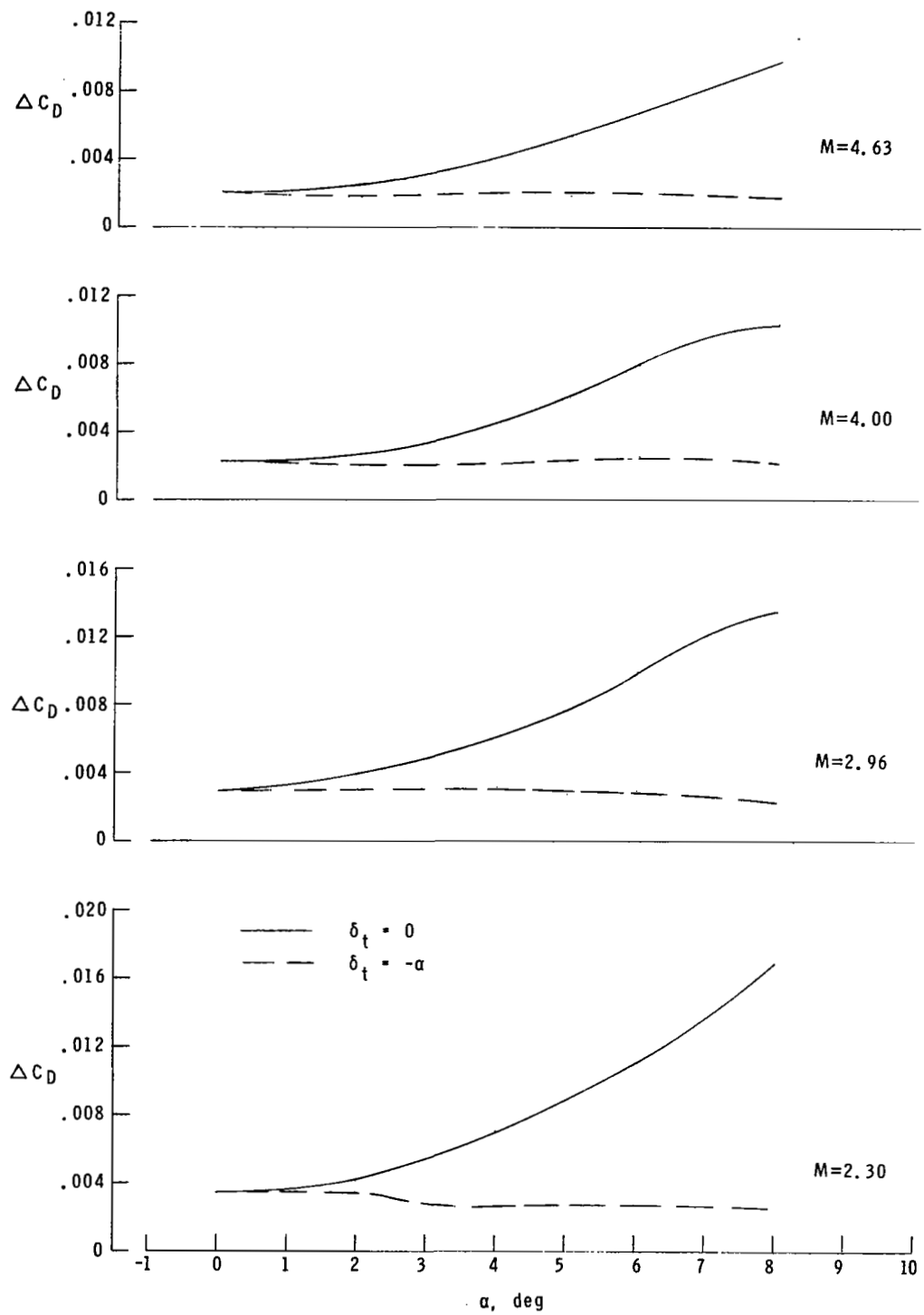

Figure 9.- Incremental drag due to horizontal tail.

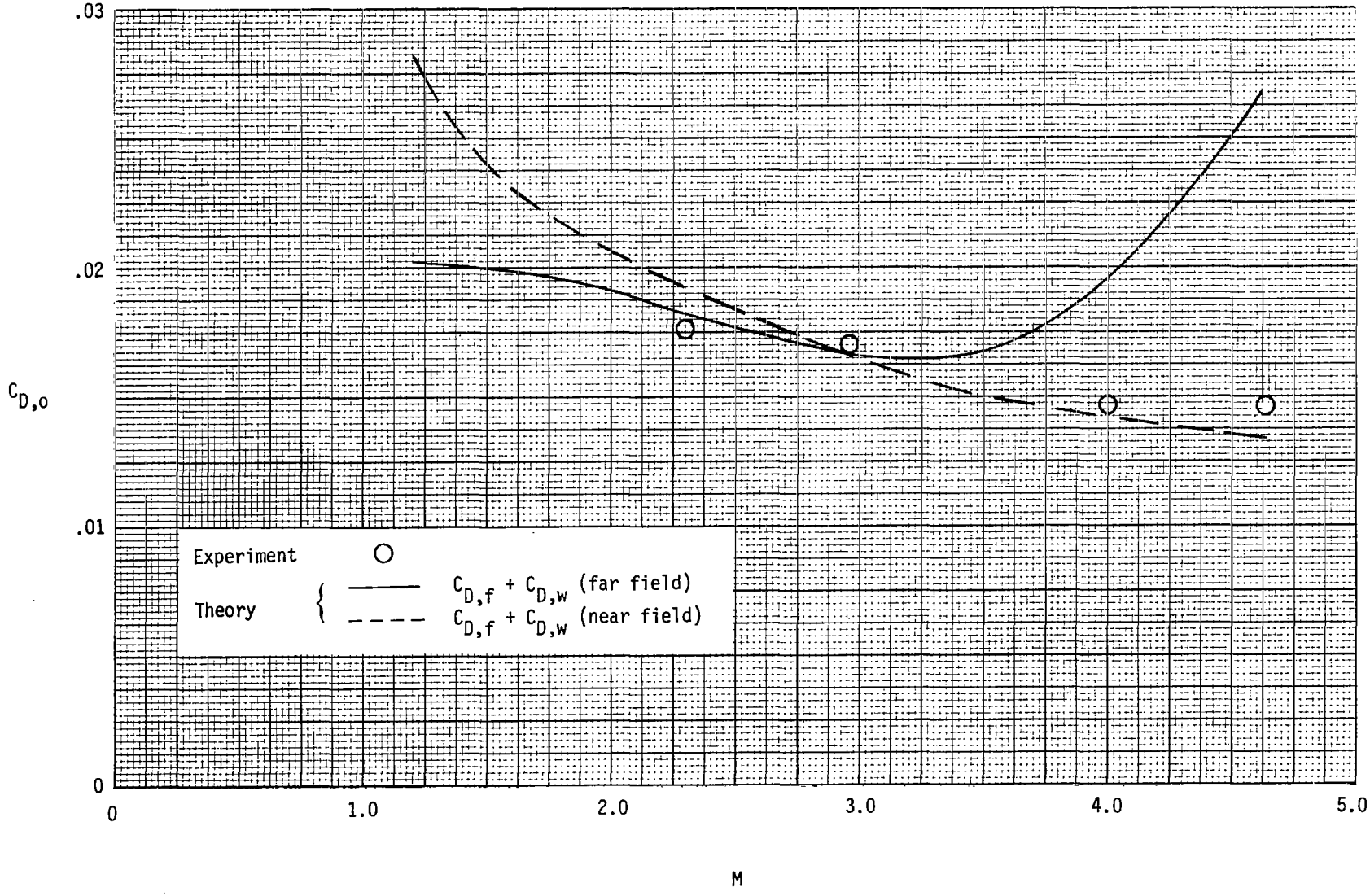

Figure 10.- Variation of theoretical minimum drag with Mach number, and comparison with experiment. Body-tail configuration; $\delta_t = 0$.

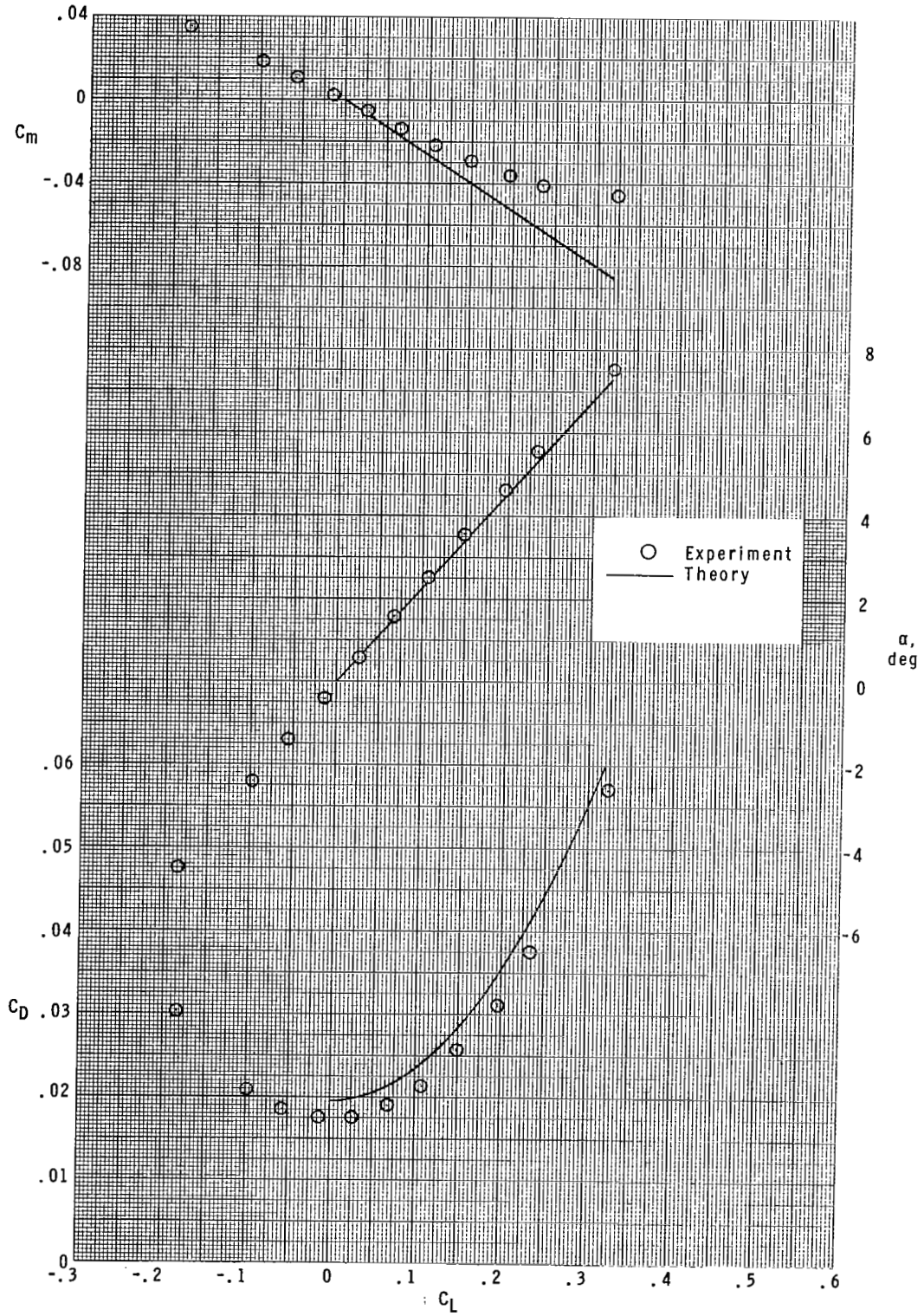

(a) M = 2.30.

Figure 11.- Comparison between experiment and theory (near-field wave-drag method) of some longitudinal aerodynamic characteristics. Body-tail configuration; $\delta_t = 0$.

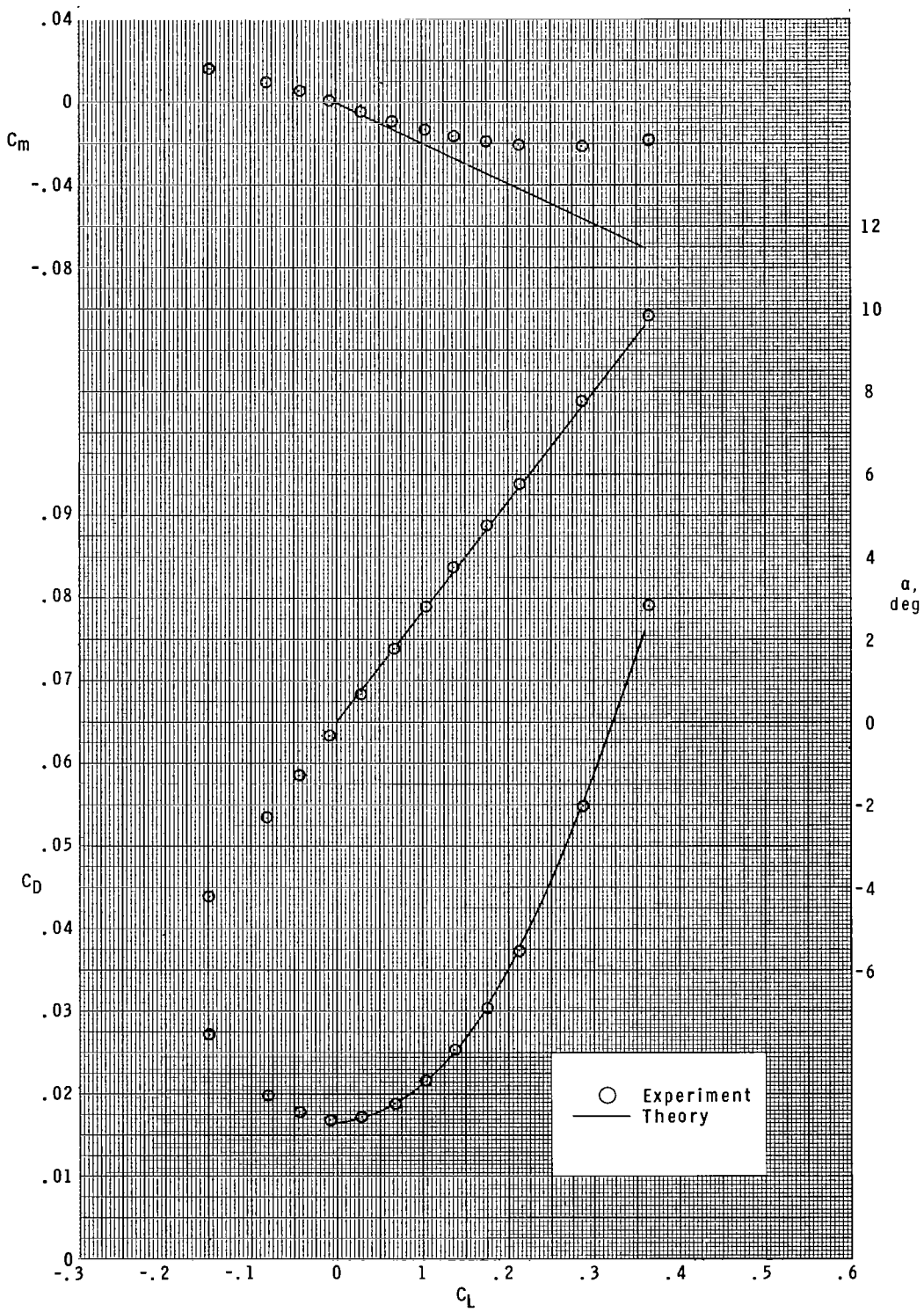

(b) M = 2.96.

Figure 11.- Continued.

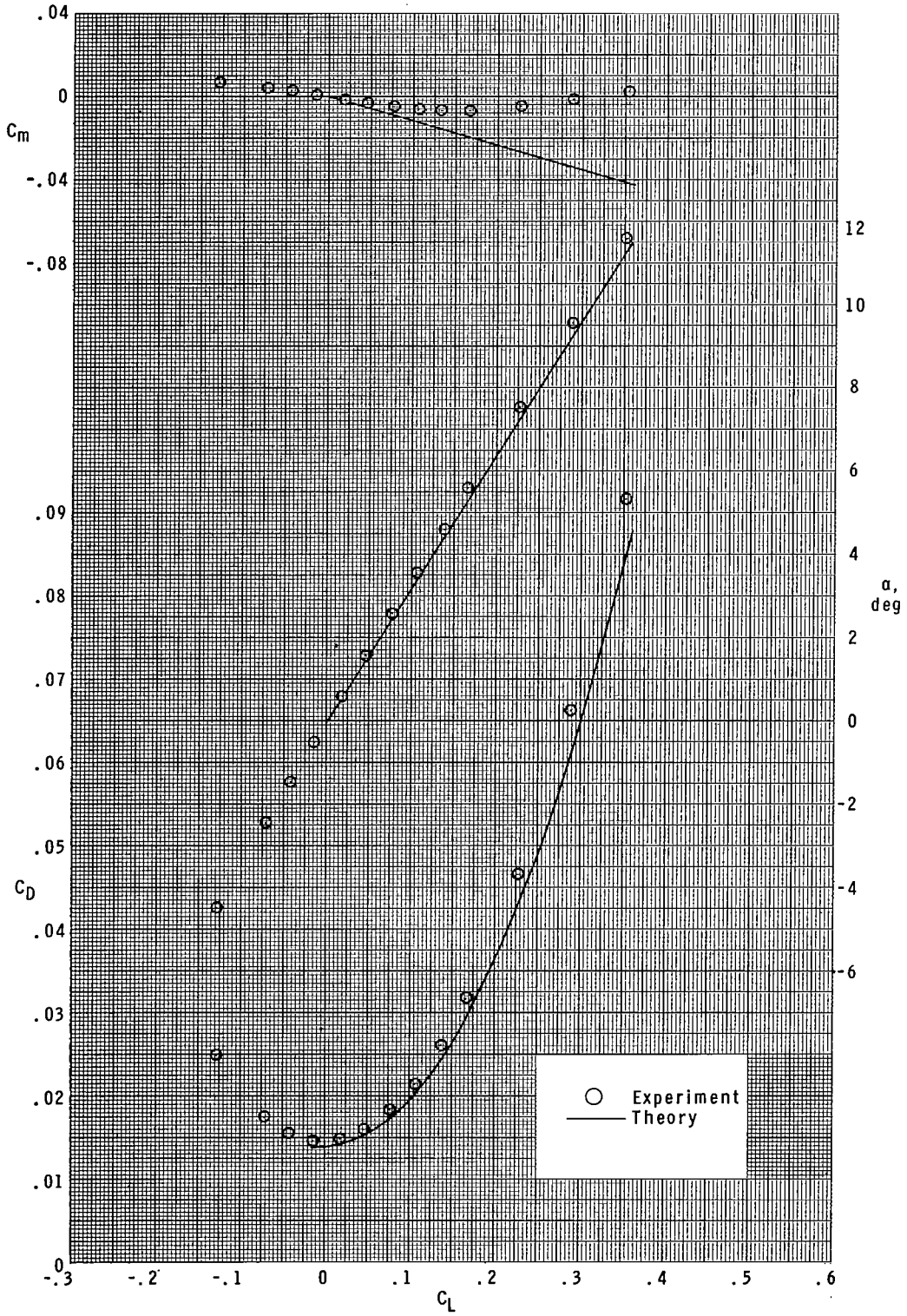

(c) M = 4.00.

Figure 11.- Continued.

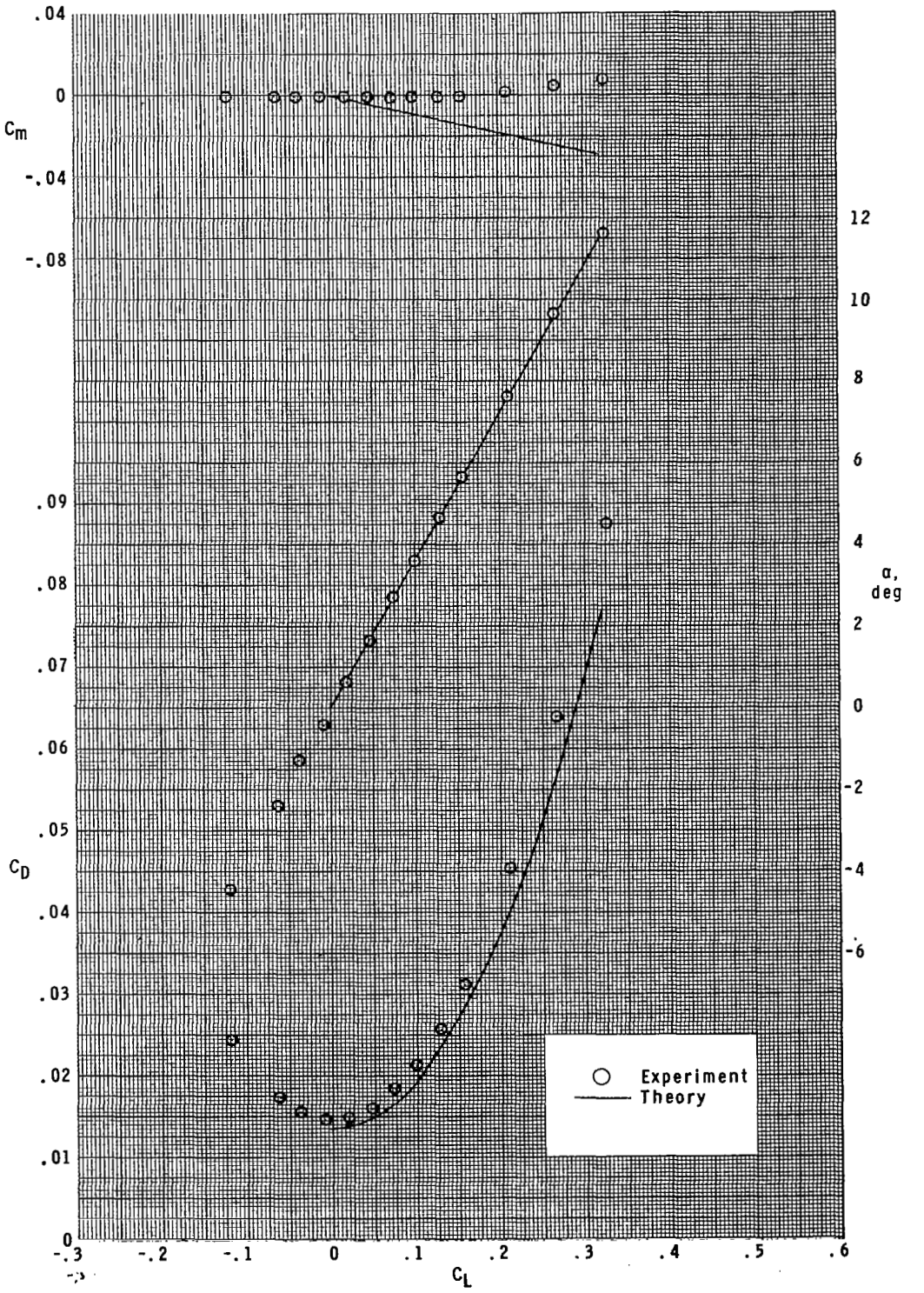

(d) M = 4.63.

Figure 11.- Concluded.

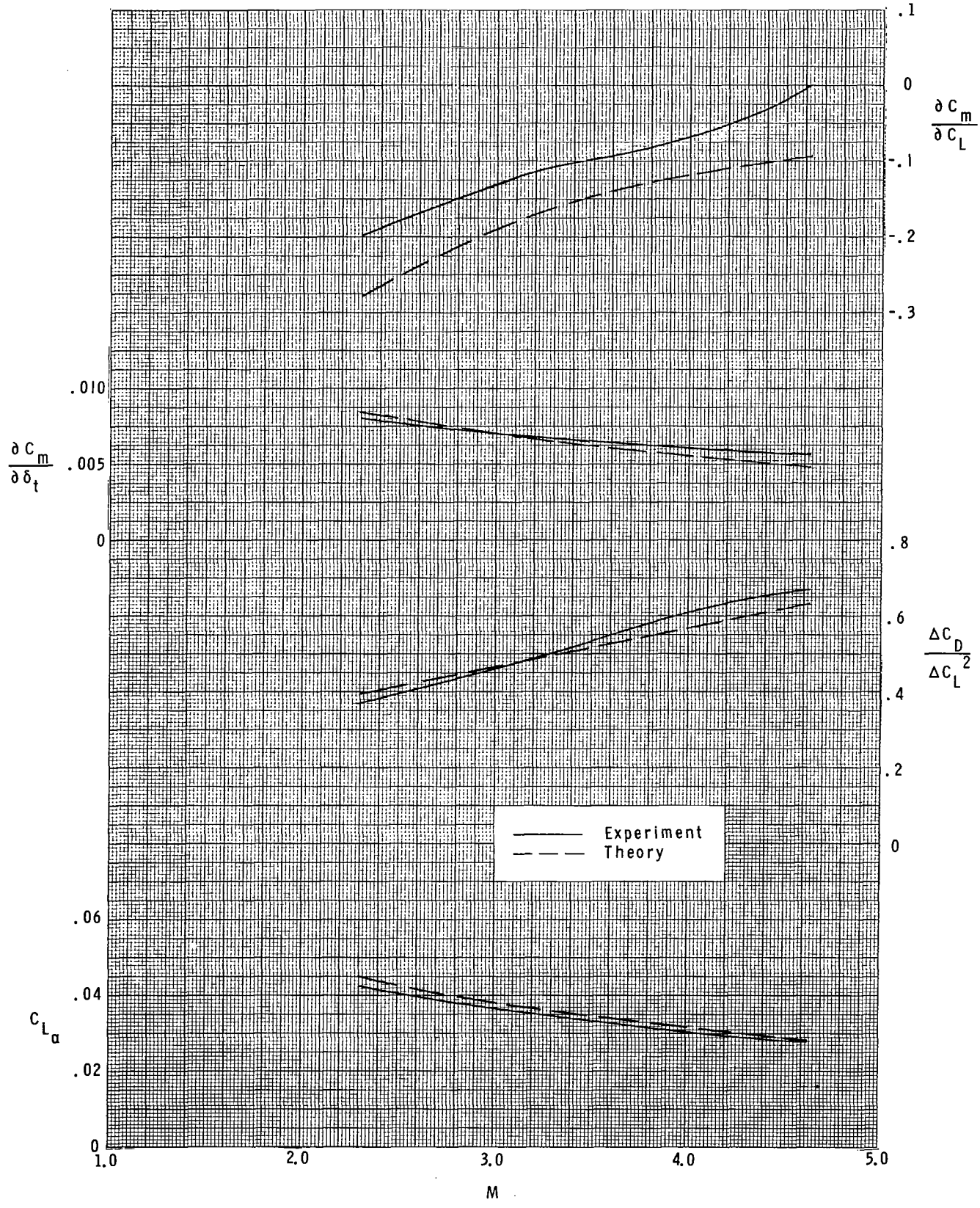

Figure 12.- Comparison between experiment and theory of the variation of some longitudinal parameters. Body-tail configuration.

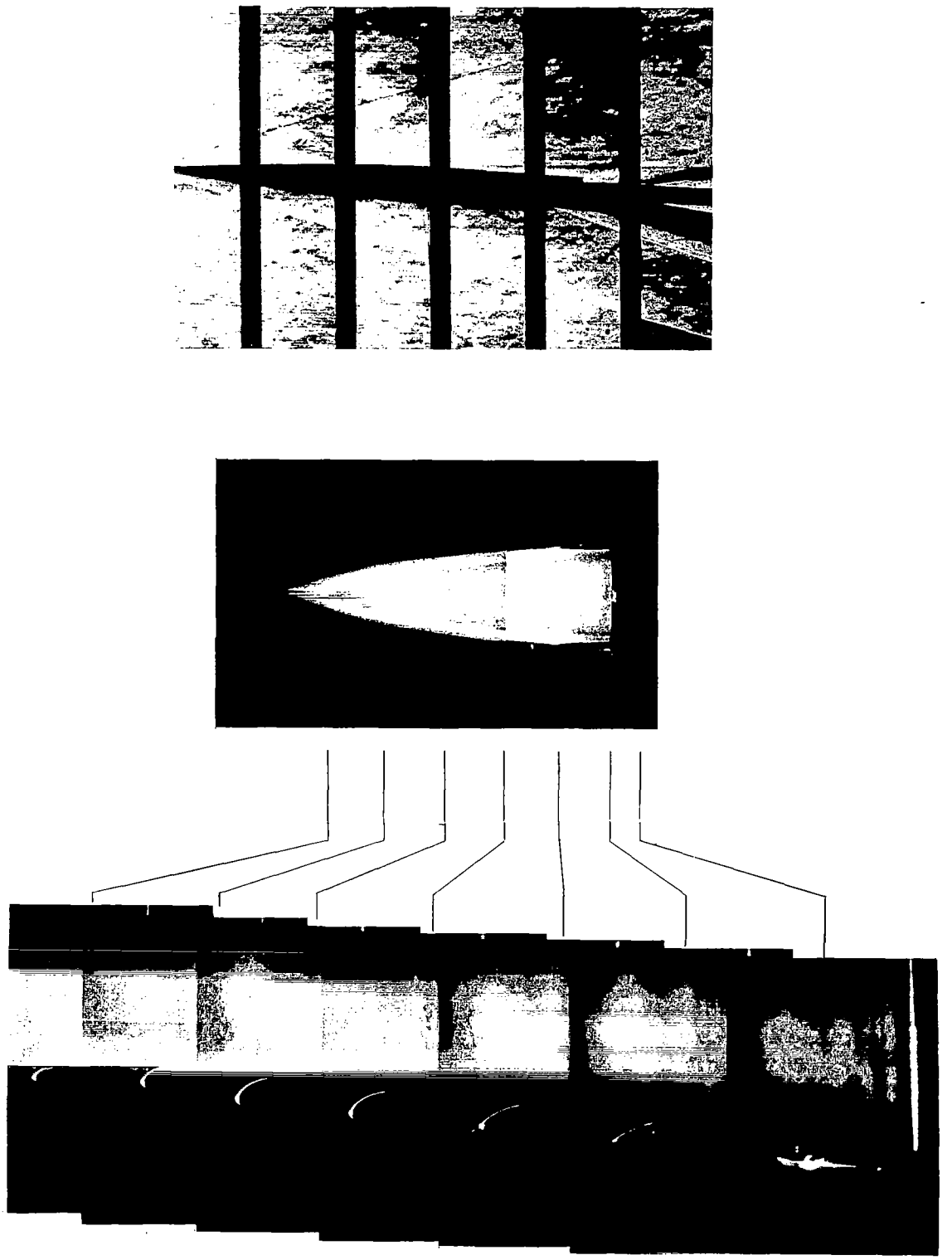

L-82-139

(a) $\alpha = 4°$.

Figure 13.- Flow visualization photographs of model. Body-tail configuration; M = 4.00.

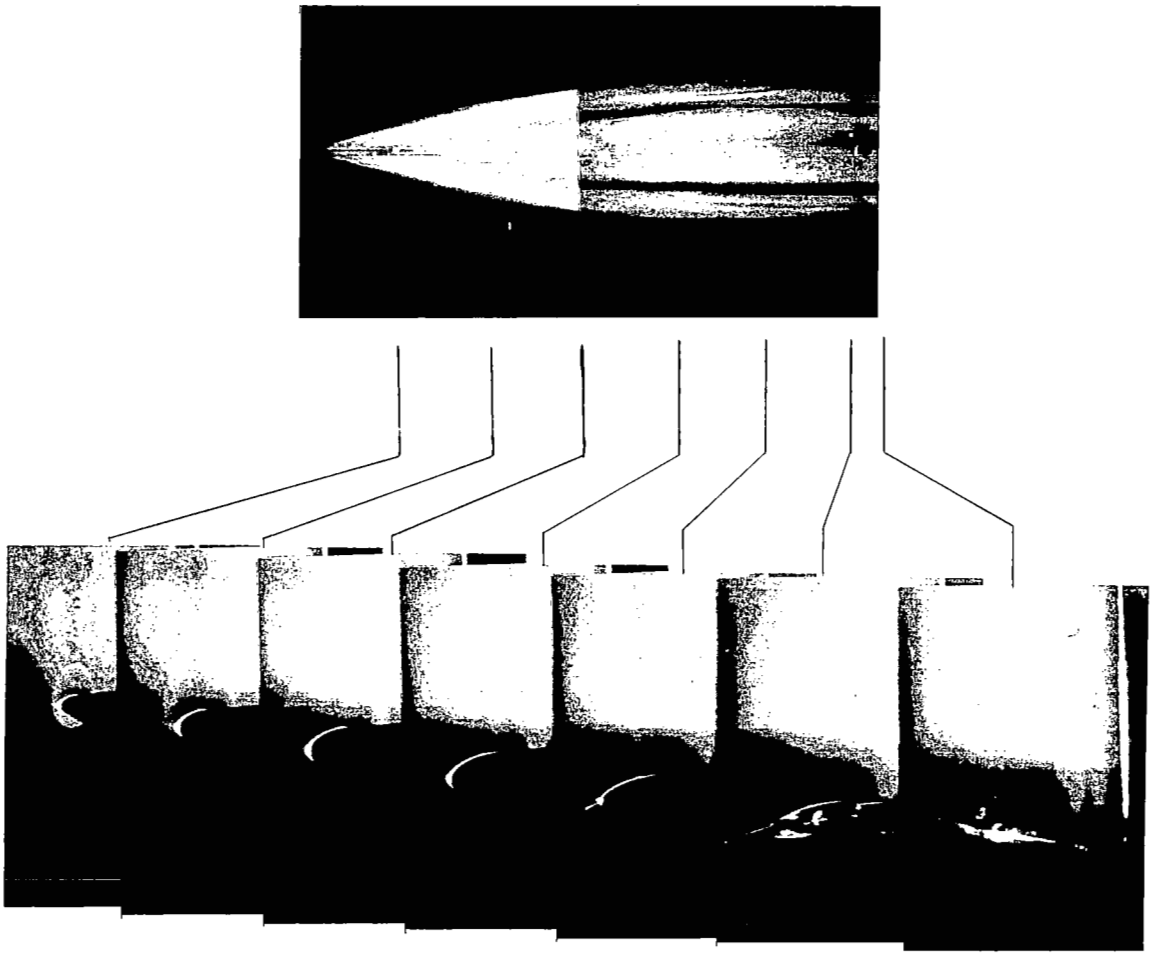

L-82-140

(b) $\alpha = 8°$.

Figure 13.- Concluded.

1. Report No.	2. Government Accession No.	3. Recipient's Catalog No.
NASA TP-2024		

4. Title and Subtitle	5. Report Date
LONGITUDINAL AERODYNAMIC CHARACTERISTICS OF AN ELLIPTICAL BODY WITH A HORIZONTAL TAIL AT MACH NUMBERS FROM 2.3 TO 4.63	June 1982
	6. Performing Organization Code 505-43-23-10
7. Author(s) Barrett L. Shrout and A. Warner Robins	8. Performing Organizatic ' Report No. L-15280
	10. Work Unit No.
9. Performing Organization Name and Address NASA Langley Research Center Hampton, VA 23665	11. Contract or Grant No.
	13. Type of Report and Period Covered Technical Paper
12. Sponsoring Agency Name and Address National Aeronautics and Space Administration Washington, DC 20546	14. Sponsoring Agency Code

15. Supplementary Notes

Barrett L. Shrout: Langley Research Center, Hampton, Virginia.
A. Warner Robins: Kentron International, Inc., Hampton, Virginia.

16. Abstract

An investigation was conducted in the Langley Unitary Plan Wind Tunnel to determine longitudinal aerodynamic characteristics of a configuration consisting of an elliptical body with an in-plane horizontal tail. The tests were conducted at Mach numbers of 2.3, 2.96, 4.0, and 4.63. In some cases, the configuration with negative tail deflections yielded higher values of maximum lift-drag ratio than did the configuration with an undeflected tail. This was due to body upwash acting on the tail and producing an additional lift increment with essentially no drag penalty. Linear theory methods used to estimate some of the longitudinal aerodynamic characteristics of the model yielded results which compared well with experimental data for all Mach numbers in this investigation and for both small angles of attack and larger angles of attack where nonlinear (vortex) flow phenomena were present.

17. Key Words (Suggested by Author(s))	18. Distribution Statement
Elliptical body Linear theory Supersonic aerodynamic characteristics Body upwash	Unclassified - Unlimited Subject Category 02

19. Security Classif. (of this report)	20. Security Classif. (of this page)	21. No. of Pages	22. Price
Unclassified	Unclassified	37	A03

For sale by the National Technical Information Service, Springfield, Virginia 22161

NASA-Langley, 1982

National Aeronautics and
Space Administration

Washington, D.C.
20546

Official Business
Penalty for Private Use, $300

THIRD-CLASS BULK RATE

Postage and Fees Paid
National Aeronautics and
Space Administration
NASA-451

NASA

POSTMASTER: If Undeliverable (Section 158 Postal Manual) Do Not Return